T. Hofmann, R. Müller, H. Andrä, J. Zausch

Numerical simulation of phase separation in cathode materials of lithium ion batteries

Berichte des Fraunhofer ITWM, Nr. 248 (2016)

ISSN 1434-9973

Bericht 248 (2016)

Die Veröffentlichungen in der Berichtsreihe des Fraunhofer ITWM können bezogen werden über:

Fraunhofer-Institut für Techno- und
Wirtschaftsmathematik ITWM
Fraunhofer-Platz 1

67663 Kaiserslautern
Germany

Telefon: +49(0)631/31600-4674
Telefax: +49(0)631/31600-5674
E-Mail: presse@itwm.fraunhofer.de
Internet: www.itwm.fraunhofer.de

Vorwort

Das Tätigkeitsfeld des Fraunhofer-Instituts für Techno- und Wirtschaftsmathematik ITWM umfasst anwendungsnahe Grundlagenforschung, angewandte Forschung sowie Beratung und kundenspezifische Lösungen auf allen Gebieten, die für Techno- und Wirtschaftsmathematik bedeutsam sind.

In der Reihe »Berichte des Fraunhofer ITWM« soll die Arbeit des Instituts kontinuierlich einer interessierten Öffentlichkeit in Industrie, Wirtschaft und Wissenschaft vorgestellt werden. Durch die enge Verzahnung mit dem Fachbereich Mathematik der Universität Kaiserslautern sowie durch zahlreiche Kooperationen mit internationalen Institutionen und Hochschulen in den Bereichen Ausbildung und Forschung ist ein großes Potenzial für Forschungsberichte vorhanden. In die Berichtreihe werden sowohl hervorragende Diplom- und Projektarbeiten und Dissertationen als auch Forschungsberichte der Institutsmitarbeiter und Institutsgäste zu aktuellen Fragen der Techno- und Wirtschaftsmathematik aufgenommen.

Darüber hinaus bietet die Reihe ein Forum für die Berichterstattung über die zahlreichen Kooperationsprojekte des Instituts mit Partnern aus Industrie und Wirtschaft.

Berichterstattung heißt hier Dokumentation des Transfers aktueller Ergebnisse aus mathematischer Forschungs- und Entwicklungsarbeit in industrielle Anwendungen und Softwareprodukte – und umgekehrt, denn Probleme der Praxis generieren neue interessante mathematische Fragestellungen.

Prof. Dr. Dieter Prätzel-Wolters
Institutsleiter

Kaiserslautern, im Juni 2001

Numerical simulation of phase separation in cathode materials of lithium ion batteries

Tobias Hofmann[a], Ralf Müller[b], Heiko Andrä[a], Jochen Zausch[a]

[a]*Department of Flow and Material Simulation, Fraunhofer Institute of Industrial Mathematics ITWM*
[b]*Department of Applied Mechanics, University of Kaiserslautern*

Abstract

Phase separation during the intercalation of lithium ions can lead to degradation effects in some cathode materials potentially, shortens life-time and decreases capacity. A nonlinear initial boundary value problem for the lithium ion concentration, the electric potential and the electrode-electrolyte interface currents is introduced on the microscale. Different exchange current densities for Butler-Volmer interface conditions are evaluated. The Cahn-Hilliard equation is used to describe the phase transition from solid-solution diffusion to two-phase dynamics. The resulting phase-field model is then discretized on a regular mesh. A first-order finite-volume scheme with adaptive time stepping is applied. The parameters and their effects in the non-convex Helmholtz energy are investigated and explained. Furthermore, the numerical convergence of the scheme is examined. In order to illustrate the method, the charging process of a complex structure is numerically simulated.

Keywords: phase-field model, Cahn-Hilliard equation, Butler-Volmer kinetics, intercalation, lithium-ion battery, finite-volume method
2010 MSC: 35K59, 65M08, 65M12, 74N25, 82B26, 82C26

1. Introduction

Today lithium ion batteries form an indispensable component for electronic devices or electric vehicles. Even though lithium ion electrodes are very versatile in battery production due to their high energy density, the diverse fields of application require the prediction of life-time, capacity fade, and the modeling of aging mechanisms. A lot of electrode materials show degradation during usage. If a large current is applied at the poles of the battery during discharge, the diffusion of lithium ions inside the battery from anode to cathode is not fast enough and concentration gradients arise. In some materials the restructuring of the lithium ions inside the crystal structure of the electrode material gives rise to large strains [3]. From experiments it is known that the stresses related to these strains can cause mechanical damage effects in materials including lithium tin oxide [5], lithium manganese oxide [15], lithium titanate oxide [6] and lithium iron phospate [7]. The mechanical stresses arising in a porous electrode made of lithium manganese oxide have been numerically simulated with a model based on diffusive dilute solution theory [25]. In this model a diffusion equation is used to describe the distribution of lithium ions inside the battery.

But especially in lithium iron phospate, the diffusion of the lithium ions from electrolyte into the active material cannot be modeled by a regular diffusion equation. While in a lot of materials the diffusion leads to an even ion distribution inside the material, for lithium iron phospate a separation into areas with a maximum concentration of lithium ions and areas where no lithium ions are present [11, 28]. Even without applied current, the lithium enriched areas do not diffuse. The distribution of the lithium ions inside the material can then be described by two different phases, one phase enriched with lithium ions and one phase devoid of lithium ions. The process of separation into different phases is called spinodal decomposition. The problem of describing the movement of the boundaries between both phases is often called a Stefan problem [1, 14] and can be approached by adaptive meshes and front-tracking methods [19].

Another approach called phase-field method is introduced in the works of Cahn and Hilliard [4] and is based on a thermodynamical approach involving a non-convex Helmholtz energy functional. In a general phase-field method, the boundary between two phases is discretized and a fine regular spatial mesh is used. In phase-field models for diffusive processes the constituent fourth-order nonlinear partial differential equation is called the Cahn-Hilliard equation. There are applications to electrode material for either spherical [27], ellipsoidal [15] or cuboid particles [2].

In Section 2 the electrochemical model for a dilute solution battery on the microscale [16] is presented. A phase-field model for phase separation given in [27] is introduced and adjusted to the electrochemical model. In Section 3 the spatial discretization and an adaptive time integration algorithm is presented. In Section 4 different numerical tests are presented. The process of spinodal decomposition is shown and explained in Subsection 4.1 on a circular cathode particle. Two different models for the exchange current density in the Butler-Volmer currents are evaluated in Subsection 4.2. In Subsection 4.3 the numerical convergence of the battery cell voltage is examined. In Subsection 4.4 the effect of the size and the shape of the cathode particle on the phase separation process is investigated. In Section 5 all findings are summarized and possible enhancements as well as extensions of the numerical method are discussed.

2. Electrochemical model

In this section the equations for a lithium ion battery model on the microscale are presented. After introducing the spatial domains involved the transport equations [16] for the lithium ions and electric charges in each domain are proposed. Current conditions on the interface between the domains are taken from established models and boundary and initial conditions complete the model. In this paper the spatial two dimensional case is considered. The extension to a three dimensional model is possible.

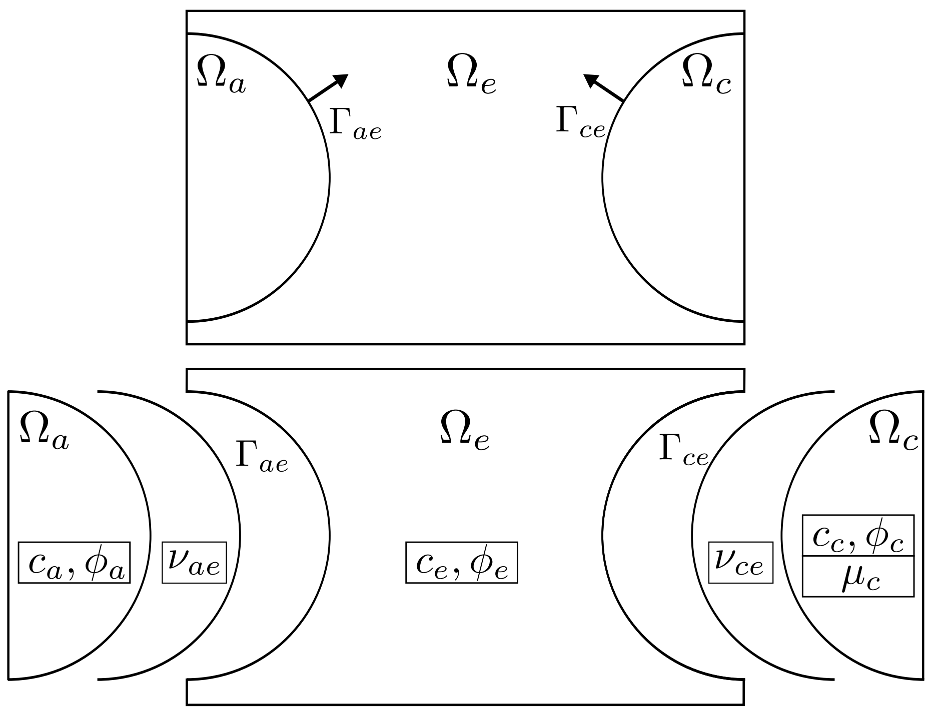

Figure 1: Decomposition of a battery cell into anode Ω_a, electrolyte Ω_e, cathode Ω_c and the interfaces Γ_{ae} and Γ_{ce}.

Name	Character	Value	Unit
Concentration	$c(x, y; t)$	-	$\mathrm{mol\,l^{-1}}$
Potential	$\phi(x, y; t)$	-	V
Universal gas constant	R	8.314	$\mathrm{J\,mol^{-1}\,K^{-1}}$
Temperature	T	300	K
Faraday constant	F	96485	$\mathrm{A\,s\,mol^{-1}}$
Lithium transference number	t_+	0.2	1
Electrolyte diffusion coefficient	D_e	$1.27 \cdot 10^{-7}$	$\mathrm{cm^2\,s^{-1}}$
Anode diffusion coefficient	D_a	10^{-10}	$\mathrm{cm^2\,s^{-1}}$
Cathode diffusion coefficient	D_c	10^{-10}	$\mathrm{cm^2\,s^{-1}}$
Electrolyte conductivity	κ_e	0.0038	$\mathrm{A\,V^{-1}\,cm^{-1}}$
Solid conductivity	κ_s	10	$\mathrm{A\,V^{-1}\,cm^{-1}}$
Maximum lithium ion concentration	c_m	20	$\mathrm{mol\,l^{-1}}$
Enthalpy of mixing per site	θ	$1.110 \cdot 10^4$	$\mathrm{J\,mol^{-1}}$
Phase-field interface energy	κ	$3.020 \cdot 10^{12}$	$\mathrm{J\,mol^{-1}\,cm^{-1}}$
Reference length	L_0	10^{-7}	cm
Anode reference potential	$\bar{U}_a$	0	V
Cathode reference potential	$\bar{U}_c$	3.42	V

Table 1: Material parameters

A rectangular domain $\Omega = (0, L_x) \times (0, L_y) \subset \mathbb{R}^2$ in Figure 1 denotes the micro-structure of a battery cell and consists of the two solid electrodes, anode Ω_a and cathode Ω_c and the liquid electrolyte Ω_e, i.e. $\Omega = \Omega_a \cup \Omega_e \cup \Omega_c$. A domain for a separator is not included in the model. The union $\Omega_s = \Omega_a \cup \Omega_c$ is called the solid domain. Figure 1 also introduces a domain decomposition with interface domains Γ_{ae}, Γ_{ce} and $\Gamma_{\mathrm{se}} = \Gamma_{ae} \cup \Gamma_{ce}$.

The equations are solved for a time interval $T = (0, t_0]$ and space-time domains are defined by $\Omega_{i,T} = \Omega_i \times T$. The function spaces $V_i = \{f : \Omega_i \to \mathbb{R}\}$ and $V_{i,T} = \{f : \Omega_i \times T \to \mathbb{R}\}$ are introduced for $i \in \{a, e, c\}$, as are $V = \{f : \Omega \to \mathbb{R}\}$ and $V_T = \{f : \Omega \times T \to \mathbb{R}\}$. Additionally on the boundaries trace spaces $W_i = \{g : \Gamma_i \to \mathbb{R}\}$ and $W_{i,T} = \{g : \Gamma_i \times T \to \mathbb{R}\}$ for $i \in \{ae, ce, se\}$ are introduced.

The following equations involve the function $c(x, y; t) \in V_T$ describing the lithium ion concentration in $\mathrm{mol\,l^{-1}}$, the function $\phi(x, y; t) \in V_T$ describing the electric potential in V and the chemical potential $\mu(x, y; t) \in V_{c,T}$ in $\mathrm{J\,mol^{-1}}$.

2.1. Governing equations

First the transport equations in the three domains $\Omega_a, \Omega_e, \Omega_c$ are introduced separately.

Electrolyte

In [16] the transport equations for ion concentration $c_e \in V_{e,T}$ and the electric potential $\phi_e \in V_{e,T}$ in an electrolyte are given as

$$\partial_t c_e - \nabla\left(D_e \nabla c_e - \frac{t_+}{z_+ F}\mathbf{j}\right) = 0, \quad (x, y; t) \in \Omega_{e,T}, \tag{1}$$

$$-\nabla\left(\kappa_e \frac{1-t_+}{z_+ F}\left(\frac{\partial \mu_e}{\partial c}\right)\nabla c_e - \kappa_e \nabla \phi_e\right) = 0, \quad (x, y; t) \in \Omega_{e,T}. \tag{2}$$

Table 1 gives numerical values for the electrolyte diffusion coefficient D_e, the electrolyte conductivity κ_e, the charge coefficient z_+, the lithium transference number t_+ and the Faraday constant F. The electric current $\mathbf{j}$ is given in [16] as

$$\mathbf{j} = \kappa_e \nabla \phi - \kappa \frac{t_+ - 1}{z_+ F}\left(\frac{\partial \mu_e}{\partial c}\right)\nabla c_e. \tag{3}$$

A logarithmically scaled chemical potential $\mu_e(c_e) = RT \log \frac{c_e}{c_m}$ is used to rewrite Eq. (1). This gives the final governing equations in terms of the concentration $c_e \in V_{e,T}$ and the electric potential $\phi_e \in V_{e,T}$ in the electrolyte as

$$\begin{aligned}\partial_t c_e - \nabla\left(\left(\frac{D_e}{RT}c_e + \frac{\kappa_e t_+(t_+ - 1)}{F^2}\right)\nabla \mu_e(c_e) + \frac{\kappa_e t_+}{F}\nabla \phi_e\right)& \\ = 0, \quad (x, y; t) \in \Omega_{e,T},& \\ -\nabla\left(\frac{\kappa_e(t_+ - 1)}{F}\nabla \mu_e(c_e) + \kappa_e \nabla \phi_e\right) = 0, \quad (x, y; t) \in \Omega_{e,T}.&\end{aligned} \tag{4}$$

This system of two equations consists of a parabolic equation and an elliptic equation [12].

Anode

An electrochemical model for the transport of lithium ions inside electrode material is taken from [16]. The continuity equation for a function $c_a \in V_{a,T}$ is

$$\partial_t c_a + \nabla \mathbf{f} = 0, \quad (x, y; t) \in \Omega_{a,T}. \tag{5}$$

The divergence of a diffusion flux $\mathbf{f}$ gives rise to local concentration changes. This flux $\mathbf{f}$ is proportional to the gradient of a chemical potential μ:

$$\mathbf{f} = D_a(c_a)\nabla \mu_a(c_a), \quad (x, y; t) \in \Omega_{a,T}. \tag{6}$$

For thermodynamic consistency, the anode diffusion coefficient $D_a(c_a)$ is chosen depending on the local lithium ion concentration c as

$$D_a(c_a) = \frac{D_0}{RT}c_a\left(1 - \frac{c_a}{c_m}\right) \tag{7}$$

The solid diffusion coefficient D_0 is smaller than in the electrolyte as diffusive processes in the solid material are more difficult than in the liquid electrolyte.

In dilute solution theory, the chemical potential is given by

$$\mu_a(c_a) = RT \log \frac{c_a}{c_m - c_a}. \tag{8}$$

It is derived from a convex Helmholtz energy assuming a maximum solid concentration c_m depending on the material [27].

Additionally the Laplace equation for an electric potential $\phi_a \in V_{a,T}$ inside the electrode is considered as

$$-\nabla(\kappa_s \nabla \phi_a) = 0, \quad (x,t) \in \Omega_{a,T}. \tag{9}$$

The electric conductivity κ_s is usually orders of magnitude larger in the electrode than in the electrolyte.

Together the aforementioned equations give the governing equations in terms of the concentration $c_a \in V_{a,T}$ and the electric potential $\phi_a \in V_{a,T}$ in the anode as

$$\begin{aligned} \partial_t c_a - \nabla\left(\frac{D_0}{RT} c_a \left(1 - \frac{c_a}{c_m}\right) \nabla \mu_a(c_a)\right) &= 0, \quad (x,y;t) \in \Omega_{a,T}, \\ -\nabla(\kappa_s \nabla \phi_a) &= 0, \quad (x,y;t) \in \Omega_{a,T}. \end{aligned} \tag{10}$$

Cathode

For the concentration $c_c \in V_{c,T}$ an extended model compared to the more simple one in the anode is considered. Instead of a logarithmic chemical potential, the chemical potential μ is defined as the variational derivative of a non-convex free energy $F(p)$ [4] in a phase-field method,

$$\frac{\mu}{RT} = \frac{\delta F(p)}{\delta p}. \tag{11}$$

The phase-field order parameter p is the normalized lithium ion concentration, $p = \frac{c}{c_m}$. In [15] the free energy is assumed as

$$\begin{aligned} F_0(p) &= H_1 + H_2, \quad \text{where} \\ H_1 &= p \log p + (1-p) \log(1-p), \\ H_2 &= \frac{\theta}{RT} p(1-p). \end{aligned} \tag{12}$$

The first term H_1 is related to a diffusion potential based on one-body terms in a Hamiltonian of the crystalline structure in active material. The second term H_2 results from a mean-field approximation of two-body interaction terms in the Hamiltonian.

The interface between lithium-rich phase and lithium-poor phase is related to misfits in the crystal structure. Therefore in phase-field methods a penalty term involving a norm of the gradient of the concentration is added to the free energy to receive

$$F(p, \nabla p) = \alpha L_0^2 \frac{G}{L} F_0(p) + \frac{\beta G L}{2} (\nabla p)^2. \tag{13}$$

The parameters G and L are introduced as an alternative description of the parameters phase-field model. They represent energy density and the width of the interfacial region, respectively. Moreover, α and β are dimensionless scalar parameters. All of these parameters are derived analytically from the representation of the free energy with the Euler-Lagrange equations in Remark 1.

From Eq. (13), the chemical potential $\mu \in V_{c,T}$ is now given as the variational derivative by

$$\frac{\mu(c_c)}{RT} = \alpha L_0^2 \frac{G}{L} F_0'(\frac{c_c}{c_m}) - \beta G L \Delta \left(\frac{c_c}{c_m}\right) \quad (x, y; t) \in \Omega_{c,T}. \tag{14}$$

Combining Eqs. (5), (6) and (14), the equations governing the lithium ion concentration $c_c \in V_{c,T}$, the electric potential $\phi_c \in V_{c,T}$ and the chemical potential $\mu \in V_{c,T}$ are given by

$$\begin{aligned} 0 &= \partial_t c + \nabla \left(\frac{D_0}{RT} c_c \left(1 - \frac{c_c}{c_m}\right) \nabla \mu \right), && (x, y; t) \in \Omega_{c,T}, \\ 0 &= -\nabla(\kappa_s \nabla \phi_c), && (x, y; t) \in \Omega_{c,T}, \\ \mu &= RT\alpha L_0^2 \frac{G}{L} F_0'(\frac{c_c}{c_m}) - RT\beta G L \Delta \left(\frac{c_c}{c_m}\right) && (x, y; t) \in \Omega_{c,T}. \end{aligned} \tag{15}$$

Here the chemical potential μ is introduced as an additional unknown. The resulting equation system for the cathode domain contains three second-order differential equations, whereas for electrolyte domain and anode domain, two second-order differential equations suffice.

Remark 1 (Derivation of the alternative phase-field representation)**.** *In this remark an alternative representation of the chemical phase-field potential μ is derived in terms of the interface width L and the interface energy density G as presented in [24].*

With the free energy F_0 in Eq. (12) *and the mixing enthalpy θ given in Table 1, the minima of the free energy can be derived from the equation $F_0'(p) = 0$ as $p_1 \approx 0.013$ and $p_2 \approx 0.987$. The corresponding concentrations are called the equilibrium concentrations $c_1 \approx 0.013\, c_m$ and $c_2 = c_m - c_1 \approx 0.987\, c_m$.*

The shifted free energy $\Delta F_0(p) = F_0(p) - F_0(p_1)$ allows to define the activation energy needed during a phase transformation from concentration p_1 to p_2 as an integral.

The coefficients in Eq. (13) *can be identified with corresponding values given in [26] as*

$$\alpha L_0^2 \frac{G}{L} = 1, \quad \beta G L = \frac{\kappa}{L_0^2 c_m N_A RT}. \tag{16}$$

With this and the use of the Euler-Lagrange equations, G and L are calculated as

$$
\begin{aligned}
G &= \frac{1}{L_0}\sqrt{2\frac{\kappa}{L_0^2 c_m N_A RT}} \int\limits_{p_1}^{p_2} \sqrt{\Delta F_0(p)} dp \approx 2.09 \cdot 10^{-7}\mathrm{cm}^{-1}, \\
L &= L_0(p_2 - p_1)\sqrt{\frac{\kappa}{2L_0^2 c_m N_A RT \Delta F_0(0.5)}} \approx 3.33 \cdot 10^{-7}\mathrm{cm}.
\end{aligned}
\tag{17}
$$

The scalar parameters α and β can now be deduced as

$$
\alpha \approx 1.593 \cdot 10^{-14}, \quad \beta \approx 1.444 \cdot 10^{10} \tag{18}
$$

The application of a phase-field method requires a fine discretization of the interface width. From the interface width being $L =$ 3.3 nm it can be concluded that the spatial discretization size should not be larger than $h \approx 1$ nm. This way the phase interface between different phases is resolved by at least three or four voxels.

Remark 2 (Equilibrium concentration)**.** *Figure 2 shows the influence of the mixing enthalpy parameter θ on the bulk chemical potential $F_0'(c)$*

$$
F_0'(c) = RT \log \frac{c}{c_m - c} + \theta \left(1 - 2\frac{c}{c_m}\right) \tag{19}
$$

in Eq. (14)*. For a value of $\theta < \theta_{crit} = 0.052\,\mathrm{kJ\,mol^{-1}}$, this chemical potential is monotonous. There are no extrema and no phase separation will occur. $\theta > \theta_{crit}$ allows phase coexistence, where the equilibrium concentration values are given by the root marks in Figure 2. An over-saturated state of charge between the equilibrium concentrations $c_1 \approx 0.013\, c_m$ and the concentration $c_s \approx 0.12\, c_m$ at the maximum S of the chemical potential gives rise to a spinodal decomposition. In this domain, small perturbations lead to phase separation into a lithium-poor phase with concentration c_1 and a lithium-rich phase with concentration $c_2 = c_m - c_1$.*

2.2. Interface conditions

The domains Γ_{ae} and Γ_{ce} in Figure 1 are both part of the electrode domain and the electrolyte domain. They act as inner boundaries between electrode and electrolyte and are called interface domains. In order to close the partial differential equations given in their respective domain, this subsection will define transmission conditions.

The trace $c_{ce,c} \in W_{ce}$ is defined as the continuous extension of $c_c \in V_{c,T}$ onto Γ_{ce}. Also, $c_e \in V_{e,T}$ and $c_a \in V_{a,T}$ are extended as $c_{ce,e}$, $c_{ae,e}$ and $c_{ae,a}$ onto Γ_{ce} and Γ_{ae}. Using the union Γ_{se} of Γ_{ce} and Γ_{ae} and the function space W_{se}, the lithium ion concentration $c_{se,s}$ can be defined as $(c_{ce,c}; c_{ae,a}) \in W_{\mathrm{se}}$ and corresponding also $c_{se,e}$ as $(c_{ce,e}; c_{ae,e}) \in W_{\mathrm{se}}$. In general $c_{se,s} \neq c_{se,e}$, i.e. there is no continuous extension of c_c and c_e across Γ_{se}. The functions ϕ_c,ϕ_e,ϕ_a are extended in the same way to functions $\phi_{se,s}$ and $\phi_{se,e}$.

Then the Butler-Volmer interface electric current $i_{\mathrm{se}} \in W_{\mathrm{se}}$ is defined as

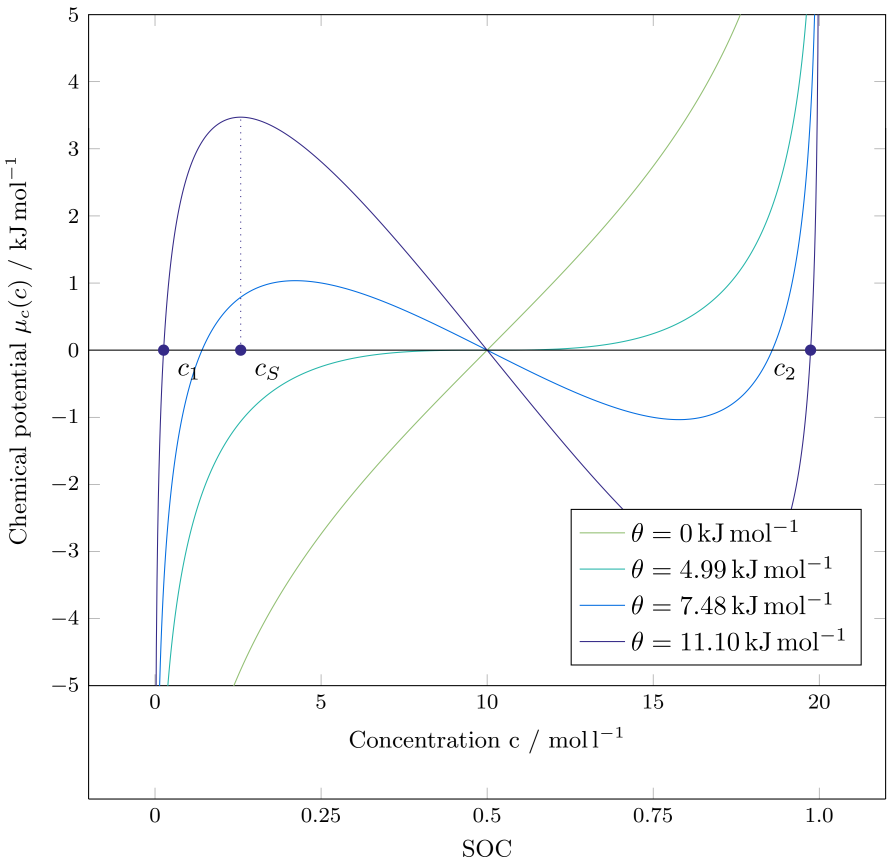

Figure 2: The bulk chemical potential $\mu_c(c)$ for different values of the phase-field enthalpy θ. Equilibrium concentrations c_1 and c_2 and local maximum S, are depicted for the value $\theta = 11.10\,\mathrm{kJ\,mol^{-1}}$.

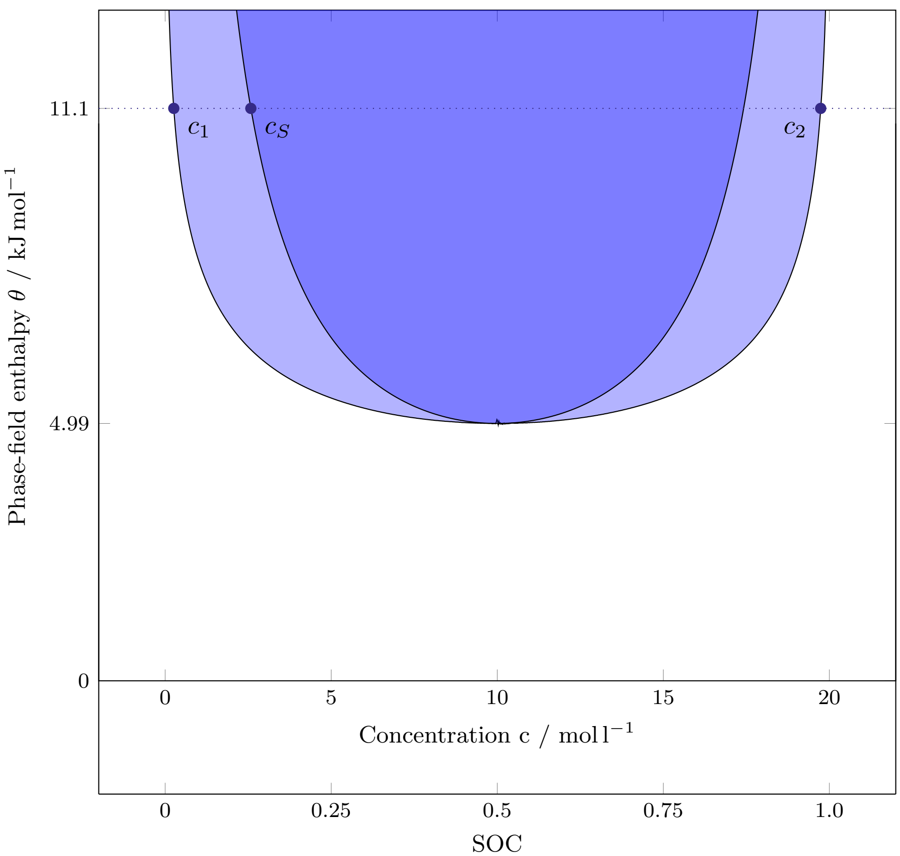

Figure 3: The phase diagram with curves denoting the equilibrium concentrations c_1 and c_2 (outer) and the point of spontaneous spinodal decomposition c_S (inner).

$$i_{\mathrm{se}} = i_0(c_{se,s}, c_{se,e}) \sinh\left(\frac{F}{2RT}\eta\right). \tag{20}$$

The function i_0 is called the exchange current density. The model introduced in [17] for the exchange current density is called Model A and is given as

$$i_0(c_{se,s}, c_{se,e}) = 2k\sqrt{c_{se,e}c_{se,s}\frac{c_m}{2}}. \tag{21}$$

In Subsection 4.2 it is compared to another model [20] called Model B given as

$$i_0(c_{se,s}, c_{se,e}) = 2k\sqrt{c_{se,e}c_{se,s}(c_m - c_{se,s})}. \tag{22}$$

The Nernst overpotential η is the difference between the electrochemical potentials on both sides of the particle surface,

$$\eta = \phi_{se,s} - \phi_{se,e} - U_0. \tag{23}$$

The open circuit potential U_0 is the difference of the chemical potential at the particle surface divided by the Faraday constant and the reference potential. U_0 is defined as

$$\begin{aligned} U_0 &= \frac{\mu_a(c_{se,s})}{F} - \bar{U}_a, \qquad && (x,t) \in \Gamma_{ae} \times T \\ U_0 &= \frac{\mu}{F} - \bar{U}_c, && (x,t) \in \Gamma_{ce} \times T \end{aligned} \tag{24}$$

The values $\bar{U}_a$ and $\bar{U}_c$ are the constant reference voltages of the electrodes given in Table 1.

The electric current i_{se} is used to define a flux boundary condition for the Laplace equations for the electric potential. To give a similar Neumann boundary condition on the diffusion equations, a corresponding interface concentration flux is defined as

$$f_{\mathrm{se}} = \frac{i_{\mathrm{se}}}{F}. \tag{25}$$

Now the interface conditions on the anode-electrolyte interface are

$$\begin{aligned} f_{\mathrm{se}} &= \mathbf{n} \cdot \left(\frac{D_0}{RT} c_{ae,a}\left(1 - \frac{c_{ae,a}}{c_m}\right) \nabla \mu_a(c_{ae,a})\right), \\ i_{\mathrm{se}} &= \mathbf{n} \cdot (\kappa_s \nabla \phi_{ae,a}), \\ f_{\mathrm{se}} &= -\mathbf{n} \cdot \left(\left(\frac{D_e}{RT} c_{ae,e} + \frac{\kappa_e t_+(t_+ - 1)}{F^2}\right) \nabla \mu_e(c_{ae,e}) + \frac{\kappa_e t_+}{F} \nabla \phi_{ae,e}\right), \\ i_{\mathrm{se}} &= -\mathbf{n} \cdot \left(\frac{\kappa_e(t_+ - 1)}{F} \nabla \mu_e(c_{ae,e}) + \kappa_e \nabla \phi_{ae,e}\right), \\ &\quad (x, y; t) \in \Gamma_{ae} \times T, \end{aligned} \tag{26}$$

and on the cathode-electrolyte interface

$$
\begin{aligned}
f_{\text{se}} =& \mathbf{n} \cdot \left(\frac{D_0}{RT} c_{ce,c} \left(1 - \frac{c_{ce,c}}{c_m} \right) \nabla \mu_{ce,c} \right), \\
i_{\text{se}} =& \mathbf{n} \cdot (\kappa_s \nabla \phi_{ce,c}), \\
f_{\text{se}} =& -\mathbf{n} \cdot \left(\left(\frac{D_e}{RT} c_{ce,e} + \frac{\kappa_e t_+ (t_+ - 1)}{F^2} \right) \nabla \mu_e(c_{ce,e}) + \frac{\kappa_e t_+}{F} \nabla \phi_{ce,e} \right), \\
i_{\text{se}} =& -\mathbf{n} \cdot \left(\frac{\kappa_e (t_+ - 1)}{F} \nabla \mu_e(c_{ce,e}) + \kappa_e \nabla \phi_{ce,e} \right), \\
& (x, y; t) \in \Gamma_{ce} \times T.
\end{aligned} \tag{27}
$$

In these definitions, the normal vector $\mathbf{n}$ is assumed to point from solid domain to electrolyte domain. The resulting transmission problem is fully coupled in all three domains. Both concentration and electric potential are involved in a nonlinear Robin condition.

2.3. Boundary and initial conditions

Since the battery cell is placed in an enclosed housing, no concentration flux over the boundaries Γ_a, Γ_c and Γ_e is possible. Therefore the boundary conditions for the concentration c are homogeneous Neumann conditions,

$$
\begin{aligned}
\alpha_s(c) \nabla \mu_a(c) &= 0, \quad (x, y; t) \in \Gamma_a \times T, \\
\alpha_e(c) \nabla \mu_e(c) + \beta \nabla \phi &= 0, \quad (x, y; t) \in \Gamma_e \times T, \\
\alpha_s(c) \nabla \mu &= 0, \quad (x, y; t) \in \Gamma_c \times T.
\end{aligned} \tag{28}
$$

Boundary conditions on the electric potential are more complex. The neutral point for the electric potential is arbitrarily assigned to the anode boundary Γ_a

$$
\phi(x, y; t) = 0, \quad (x, y; t) \in \Gamma_a \times T. \tag{29}
$$

The parameter C rate is used to define meaningful charging boundary conditions. It is defined as quotient of charging current and battery capacity and usually specified in the unit h^{-1}. C rate 1 defines a charging current i_{in} such that it takes one hour to charge the battery cell from empty to full state of charge. On the cathode boundary Γ_c a constant current density i_{in} is applied such that a particular C rate is achieved,

$$
\kappa_s \nabla \phi(x, y; 0) = i_{\text{in}}, \quad (x, y; t) \in \Gamma_c \times T. \tag{30}
$$

The boundary Γ_e containing the electrolyte is assumed to be an isolating material with no electric current permitted,

$$
\left(\frac{D_e}{RT} c_{ce,e} + \frac{\kappa_e t_+ (t_+ - 1)}{F^2} \right) \nabla \mu_e(c_{ce,e}) + \frac{\kappa_e t_+}{F} \nabla \phi_{ce,e} = 0, \quad (x, y; t) \in \Gamma_e \times T. \tag{31}
$$

In Eq. (15) for the chemical potential μ in the cathode material, the boundary condition on the interface $\Gamma_{ce,c}$ is equivalent to the abundance of a surface wetting effect.

$$\partial_n c = 0, \quad (x, y; t) \in (\Gamma_c \cup \Gamma_{ce}) \times T. \tag{32}$$

If not noted otherwise, the initial lithium ion concentration in the respective domains is prescribed as

$$\begin{aligned}
c(x, y; 0) &= 0.99 c_m, && (x, y) \in \Omega_a, \\
c(x, y; 0) &= 0.06 c_m, && (x, y) \in \Omega_e, \\
c(x, y; 0) &= 0.01 c_m, && (x, y) \in \Omega_c.
\end{aligned} \tag{33}$$

This corresponds to the state of charge $SOC = 0.99$ in the anode and $SOC = 0.01$ in the cathode. Consistent initial values for the electric potential and the particle surface currents can now be calculated

$$\begin{aligned}
\phi(x, y; 0) &= \phi_0(x, y), && (x, y) \in \Omega, \\
i(x, y; 0) &= i_0(x, y), && (x, y) \in \Gamma_{\mathrm{se}}.
\end{aligned} \tag{34}$$

3. Numerical method

Phase-field models on periodic domains have been extensively studied and solved with methods using fast Fourier transformation [23, 24]. Problems on active material particles with a constant Butler-Volmer currents as a boundary condition have been simulated with higher-order schemes due to the fourth-order Cahn-Hilliard equation in order to make use of larger time steps [27, 9]. However, the highly nonlinear interface conditions in combination require small time-steps regardless of the convergence order of the scheme used. For this reason a first-order scheme in time is applied. Even though unconditionally stable semi-implicit backwards schemes have successfully been derived and proved for the simple elliptic equations and Cahn-Hilliard equations in [13], they are not capable of implementing nonlinear interface conditions. Therefore a fully-implicit scheme is applied.

For the spatial discretization of diffusion problems, finite-volume methods have prover to be useful and flexible. The electrochemical model in Section 2 describes interface fluxes which can be incorporated in a finite-volume scheme on cell centers. The spatial discretization presented here is similar to the one used in [22]. A uniform regular cell grid is used and thus a finite-volume scheme on cell-centered voxels is identical to a finite-difference scheme [18].

In this section, a general first-order, finite-volume, cell-centered scheme for discretizing a parabolic differential equation with nonlinear conductivity coefficients and interface conditions is explained. Variables for the concentration, the electric potential and the interface fluxes are introduced.

$\tilde{\mu}(\tilde{c}) = \frac{1}{RT}\mu(c_m\tilde{c})$	$\tilde{c} = \frac{c}{c_m}$	$\tilde{\phi} = \frac{F}{RT}\phi$
$\tilde{t} = \frac{D_e}{L_x^2}t$	$\tilde{i} = \frac{i}{i_{\text{in}}}$	$\tilde{x} = \frac{x}{L_x}$

Table 2: Non-dimensionalization of variables

3.1. Non-dimensionalization

Table 2 shows dimensionless variables with tildes. For the non-dimensionalization the universal gas constant R, the temperature T, the Faraday constant F, the maximum lithium ion concentration in the solid material c_m, the diffusivity in the electrolyte D_e and the current density i_{in} given in the boundary condition. The size of the domain in the first dimension L_x is applied as a reference length. This enables us to describe both spatial and time derivatives in the following way:

$$\begin{aligned} \frac{\partial}{\partial \tilde{x}_i} &= L_x \frac{\partial}{\partial x_i} \\ \tilde{\nabla} &= L_x \nabla \\ \frac{\partial}{\partial \tilde{t}} &= \frac{D_e}{L_x^2}\frac{\partial}{\partial t} \end{aligned} \tag{35}$$

For the subsequent derivation dimensionless equations are utilized without explicit usage of the tilde notation.

3.2. Mesh

Suppose that N_x and N_y are positive integers such that $\frac{L_x}{N_x} = \frac{L_y}{N_y}$. Let $h := \frac{L_x}{N_x}$ and consider a uniform mesh Ω_h on Ω, defined by

$$\begin{aligned} \Omega_h := \{(x, y) \in \mathbb{R}^2 | x = ih - \frac{1}{2}, y = jh - \frac{1}{2} \\ 1 \leq i \leq N_x, 1 \leq j \leq N_y\}. \end{aligned} \tag{36}$$

Let $N := |\Omega_h| = N_x N_y$ and let V_h denote the linear space of real-valued functions defined on Ω_h. Meshes $\Omega_{i,h} = \Omega_i \cap \Omega_h$ are defined for $i \in \{a, e, c\}$.

Consider a second mesh Σ_h on Ω, defined by

$$\begin{aligned} \Sigma_h :=& \{(x, y) \in \mathbb{R}^2 | x = ih, y = jh - \frac{1}{2} \\ & 0 \leq i \leq N_x, 1 \leq j \leq N_y\} \cup \\ & \{(x, y) \in \mathbb{R}^2 | x = ih - \frac{1}{2}, y = jh, \\ & 1 \leq i \leq N_x, 0 \leq j \leq N_y\} \end{aligned} \tag{37}$$

Let $N_{\text{f}} := |\Sigma_h| = (N_x + 1)N_y + N_x(N_y + 1)$ and let W_h denote the linear space of real-valued functions defined on Σ_h. A partition of Σ_h into different meshes is now defined.

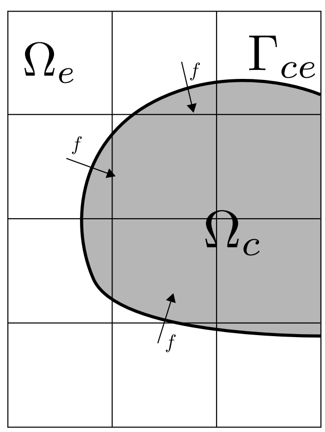

(a) A continuous structure depicting the cathode-electrolyte interface in a battery. The electrolyte domain Ω_e and the cathode domain Ω_c are co-incide at the interface domain Γ_{ce}. The concentration flux f flows into the cathode particle.

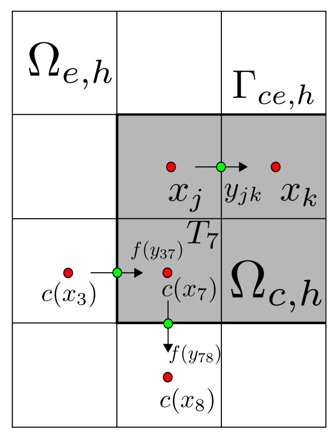

(b) A discretization of the structure into finite volume cells with a mesh $\Omega_h = \{x_i\}$ in the cell centers (red) and a shifted mesh $\Sigma_h = \{y_i\}$ on the edges of the cells (green). The components c_i of a function $c_h \in V_h$ discretize the lithium ion concentration. Components f_i of a function $f \in W_h$ discretize the concentration flux.

Figure 4: Discretization of a battery structure

Figure 4 shows both Ω_h and the shifted mesh Σ_h. Also a notation relating elements of Σ_h to elements of Ω_h is established. The mesh Σ_h is the union of several meshes $\Sigma_{i,h}$ for $i \in \{a, c, e\}$ and $\Gamma_{i,h}$ for $i \in \{ae, ce, a, e, c\}$. A mesh point y_{jk} is considered an element of $\Sigma_{i,h}$, if it lies on the edge between two cells T_j and T_k with center points x_j and x_k being elements of the $\Omega_{i,h}$,

$$\Sigma_{i,h} = \{y_{jk} \in \Sigma_h | x_j, x_k \in \Omega_{i,h}\} \quad \text{for} \quad i \in \{a, c, e\}. \tag{38}$$

Mesh points y_{jk} on edges between two cells T_j and T_k with x_j being an element of a discretized solid domain $\Omega_{a,h} \cup \Omega_{c,h}$ and x_k being an element of the discretized electrolyte domain $\Omega_{e,h}$ are considered elements of domain $\Gamma_{ae,h}$,

$$\begin{aligned} \Gamma_{ae,h} &= \{y_{jk} \in \Sigma_h | x_j \in \Omega_{a,h}, x_k \in \Omega_{e,h}\}, \\ \Gamma_{ce,h} &= \{y_{jk} \in \Sigma_h | x_j \in \Omega_{c,h}, x_k \in \Omega_{e,h}\}. \end{aligned} \tag{39}$$

The remaining mesh points y_{jk} are considered elements of $\Gamma_{i,h}$ for $i \in \{a, c, e\}$ as they lie on the boundary of Ω.

Each cell center x_j in Ω_h is now related to four edge nodes y_{jk} in Σ_h. A function in V_h can be considered an element of V by a cell-wise constant projection.

3.3. Finite volume discretization

The governing equations are discretized depending on two functions $f, i \in W_h$ called the concentration flux and the electrical current. The discretization is demonstrated by the diffusion equation in the anode, but respective steps are taken for the remaining diffusion equations, the Laplace equations for the electric potential and the equation for the chemical potential μ in the cathode.

Let $\bar{c} \in V_{a,T}$ a solution for the lithium ion concentration in Eq. (10), τ the current time step size and $t > \tau$ a fixed time. Then $c = \bar{c}(\cdot; t) \in V$ is called the current solution and $\check{c} = \bar{c}(\cdot; t - \tau) \in V$ is called the previous solution. Integration of the diffusion equation in Eq. (10) over $[t - \tau, t]$ gives

$$\begin{aligned} 0 &= \int\limits_{t-\tau}^{t} \partial_t \bar{c} dt - \int\limits_{t-\tau}^{t} \nabla \left(\frac{D_0}{RT} \bar{c} \left(1 - \frac{\bar{c}}{c_m} \right) \nabla \mu_a(\bar{c}) \right) dt = \\ &= c - \check{c} - \tau \nabla \left(\frac{D_0}{RT} c \left(1 - \frac{c}{c_m} \right) \nabla \mu_a(c) \right) + O(\tau). \end{aligned} \tag{40}$$

Now an integral in space over Ω is discretized into cubic cells T_j surrounding mesh points $x_j \in \Omega_h$. With the divergence theorem, the volume integrals are converted into surface integrals. Given $c_h \in V_h$ and $c_{h,j} := c_h(x_j)$, it is

$$
\begin{aligned}
0 &= \int_{T_j} (c - \check{c}) dV - \tau \int_{T_j} \nabla \left(\frac{D_0}{RT} c \left(1 - \frac{c}{c_m}\right) \nabla \mu_a(c) \right) dV + O(\tau) \Leftrightarrow \\
0 &= \int_{T_j} (c - \check{c}) dV - \tau \int_{\partial T_j} \left(\frac{D_0}{RT} c \left(1 - \frac{c}{c_m}\right) \nabla \mu_a(c) \right) dS + O(\tau) \Leftrightarrow \\
0 &= h^3 (c_{h,j} - \check{c}_{h,j}) - h^2 \tau \sum_{y_{jk} \in \Sigma_h} f_{jk} + O(h + \tau) \quad \forall x_j \in \Omega_h.
\end{aligned}
\tag{41}
$$

Components of $f \in W_h$ between two cells T_j and T_k in the same domain such that $y_{jk} \in \Sigma_{a,h}$ are approximated first order by

$$
\begin{aligned}
f_{jk} &= \frac{D_0}{RT} c \left(1 - \frac{c}{c_m}\right) \nabla \mu_a(c) = \\
&= \frac{D_0}{RT} \frac{c_{h,j} + c_{h,k}}{2} \left(1 - \frac{c_{h,j} + c_{h,k}}{2c_m}\right) \frac{\mu_a(c_{h,j}) - \mu_a(c_{h,k})}{h} + O(h) \\
&\text{if } f_{jk} \in \Sigma_{a,h}.
\end{aligned}
\tag{42}
$$

The next subsection defines the remaining components of the flux $f \in W_h$ by defining components $f_{jk} := f(y_{jk})$ for $y_{jk} \in \Gamma_{i,h}$ for $i \in \{ae, ce, a, c, e\}$.

The cell-wise constant projection of c_h and ϕ_h from V_h onto V defines the continuous extension of lithium ion concentration and electric potential onto $\Gamma_{ae,h}$ and $\Gamma_{ce,h}$. If $x_j \in \Omega_{c,h}$ and $x_k \in \Omega_{e,h}$ the discretized electric current i_{jk} between the cells T_j and T_k is approximated with Eq. (20) and Eq. (23) as

$$
i_{jk} = i_0(c_{h,j}, c_{h,k}) \sinh \left(\frac{F}{2RT} \eta(\phi_{h,j}, \phi_{h,k}, \mu_{h,j}) \right) + O(h + \tau), \tag{43}
$$

and respectively for $x_j \in \Omega_{a,h}$ and $x_k \in \Omega_{e,h}$. The chemical potential μ is taken from the previous iteration step and convergence is achieved by a fixed point iteration. Components of the concentration flux f_{jk} are defined accordingly.

The remaining components f_{jk} of the discretized concentration flux $f \in W_h$ are zero for $y_{jk} \in \Gamma_{a,h} \cup \Gamma_{e,h} \cup \Gamma_{c,h}$ according to the boundary conditions in Eq. (28). The components i_{jk} of the discretized electrical current $i \in W_h$ are zero for $y_{jk} \in \Gamma_{e,h}$ according to Eq. (31) and identical to i_{in} for $y_{jk} \in \Gamma_{c,h}$ according to Eq. (30). For $y_{jk} \in \Gamma_{a,h}$, components i_{jk} are set such that the Dirichlet boundary condition in Eq. (29) is fulfilled. Finally the components defining the gradient of the lithium ion concentration ∇c in Eq. (15) for the chemical potential μ in the cathode are also set according to the surface wetting boundary condition in Eq. (32).

The initial conditions in Eq. (33) are evaluated at $x_j \in \Omega_h$ to get the initial configuration $c_h \in V_h$ at time $t = 0$ as

$$
c_{h,j} = c(x, y; 0), \quad x_j \in \Omega_h. \tag{44}
$$

step $\leftarrow 0$;
$t \leftarrow 0$;
while *true* **do**
    SOC $\leftarrow$ Calculate state of charge;
    if $SOC > \overline{SOC}$ **then** Finish simulation;
    $u_0 \leftarrow \check{u}$;
    for k=1.. **do**
        if $k > k_{max}$ **then**
            $\tau \leftarrow \frac{\tau}{2}$;
            Restart time step;
        end if
        $e \leftarrow$ Calculate error of u_{k-1};
        if $e < \epsilon$ **then**
            $u \leftarrow u_{k-1}$;
        else
            f, $J \leftarrow$ Calculate residuum and Jacobian from u_{k-1};
            $d \leftarrow$ Calculate search direction from J and f;
            $u_k \leftarrow$ Calculate new Newton iterate of u_{k-1} and d;
        end if
    end for
    $t \leftarrow t + \tau$;
    step $\leftarrow$ step + 1;
    if *step-lastDampedStep* $> N_{trust}$ **then** $\tau \leftarrow \min(\tau_{\max}, 2\tau)$; ;
end while

Algorithm 1: Time-adaptive damped Newton-Raphson scheme

3.4. Linearization and adaptive algorithm

In the previous subsection the electrochemical model is discretized and the following nonlinear system of equations is established. At each time step a solution of this system is required. In this subsection a damped Newton-Raphson algorithm with an adaptive time step algorithm is introduced.

$$
\begin{aligned}
0 &= h^3(c_{h,j} - \check{c}_{h,j}) - h^2\tau \sum_{y_{jk}\in\Sigma_h} f_{jk}(c_h,\phi_h), && \forall x_j \in \Omega_h,\\
0 &= -h^2 \sum_{y_{jk}\in\Sigma_h} i_{jk}(c_h,\phi_h), && \forall x_j \in \Omega_h,\\
i_{jk} &= i_0(c_{h,j},c_{h,k})\sinh\left(\frac{F}{2RT}\eta(\phi_{h,j},\phi_{h,k},\check{\mu}_{h,k})\right), && \forall y_{jk} \in \Gamma_{ae,h}\cup\Gamma_{ce,h}.
\end{aligned}
\tag{45}
$$

The discretization for the equation for the chemical potential μ is an explicit expression in c_h. Therefore μ is eliminated from the equations. Define $N_{ae} = |\Gamma_{ae,h}|$, $N_{ce} = |\Gamma_{ce,h}|$ and $N_{\mathrm{se}} = N_{ae} + N_{ce}$. The discretized system in Eq. (45) involves N equations given by the discretized diffusion equation, N equations given by the discretized Laplace equation and N_{se} equations given by the equation defining the particle surface flux. Then the number of degrees of freedom of the equation system is $N_{DoF} = N + N + N_{\mathrm{se}}$.

Eq. (45) is written as $f(u) = 0$. The vector $u \in \mathbb{R}^{N_{\mathrm{DoF}}} \cong V_h \times V_h \times W_h$ is called solution vector and is defined as $u = (c_h;\phi_h;i_h) \in \mathbb{R}^{N_{\mathrm{DoF}}}$. Introducing terms of a general nonlinear equation solver, $f = f(u)$ is called the residuum and $J = Df(u) \in \mathbb{R}^{N_{\mathrm{DoF}}\times N_{\mathrm{DoF}}}$ is called the Jacobian matrix of the system. The Newton direction vector $d \in \mathbb{R}^{N_{\mathrm{DoF}}}$ is the solution to the linear equation system given by $Jd = f$.

Algorithm 1 defines a time-adaptive damped Newton-Raphson scheme and Algorithm 2 defines a line search scheme. The index k denotes the current Newton iteration. The index l denotes the current line search iteration. The error e corresponds to discrete L^2-norms for the grid functions c_h, ϕ_h and i_h and is calculated as

$$
||f||_2 = \sqrt{h^3\sum_{j=1}^{N} c_{h,j}^2} + \sqrt{h^3\sum_{j=1}^{N} \phi_{h,j}^2} + \sqrt{h^2\sum_{j=1}^{N_{\mathrm{se}}} i_{h,j}^2}. \tag{46}
$$

The line search in Algorithm 2 ensures global linear convergence and local quadratic convergence [21]. If a lot of sequential undamped Newton iterations are accepted the time step is enlarged. Corresponding, the time step is reduced if the Newton iteration takes too many steps. Table 3 defines the parameters used in the solver. Possible extensions include an arc-length scheme for finding an optimum time step size [8].

An iteration on a smaller nonlinear equation system with size $N_{\mathrm{steady}} := N + N_{\mathrm{se}}$ given by the equations in ϕ_h and i_{jk} is used in a first iteration step to establish consistent values for the electric potential and the particle surface

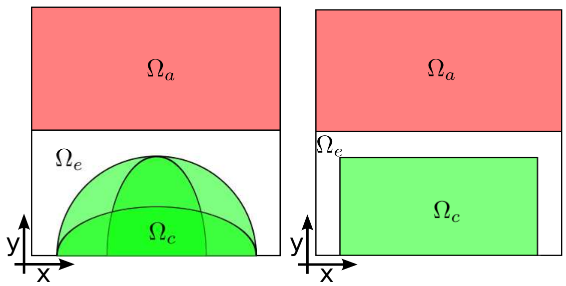

Figure 5: Structures containing cathode particle domains in the shape of different ellipsoids (left) and a rectangle (right)

current. For this iteration an undamped Newton algorithm is applied. The electric potential ϕ_h is initialized on $\Omega_{a,h}$, $\Omega_{e,h}$ and $\Omega_{c,h}$ with the values 0, $\bar{U}_a$ and $\bar{U}_a + \bar{U}_c$, respectively and the particle surface current i_{jk} on $\Gamma_{ae,h}$ and $\Gamma_{ce,h}$ is initialized with values proportional to the boundary current density i_{in}.

Data: Current Newton iterate u_{k-1}, search direction d, current residual error e
Result: New Newton iterate u_k
for $l = 1..$ **do**
    $u_{k,l} \leftarrow u_{k-1} - \omega_{l-1} d$;
    Project concentration in $u_{k,l}$ to feasible domain;
    $\bar{e} \leftarrow$ Calculate new error of $u_{k,l}$;
    if $\bar{e} < e$ **then**
        $u_k = u_{k,l}$;
        Return;
    else if $\omega > \omega_{min}$ **then**
        lastDampedStep $\leftarrow$ step;
        $\omega_l \leftarrow \omega_{l-1}\sigma$;
    else if $\tau > \tau_{min}$ **then**
        $\tau \leftarrow \frac{\tau}{2}$;
        Restart time step;
    end if
end for

Algorithm 2: Line search in the adaptive damped Newton-Raphson scheme

3.5. Numerical convergence

In this section the numerical convergence of the presented method is examined. In Figure 5 a microstructure made of anode, electrolyte and a cathode particle with rectangular shape is shown. This rectangular shape is chosen such that the resulting discretization is independent of the spatial discretization

Name	Symbol	Value
Number of undamped steps until time step is doubled	N_{trust}	10
Maximum state of charge	$\overline{SOC}$	0.99
Error criterion	ϵ	10^{-10}
Maximum number of Newton iterations	$k_{\max}$	20
Reduction factor in the line search algorithm	σ	$\frac{1}{2}$
Initial line search step size	ω_0	1
Minimum line search step size	$\omega_{\min}$	10^{-3}
Minimum time step size	$\tau_{\min}$	10^{-6}
Maximum time step size	$\tau_{\max}$	$\frac{t_0}{100}$

Table 3: Parameters for the time integration scheme

width h. A domain with width and height 50 nm and the interface width and interface energy density given in Table 1 are used. The initial state of charge SOC in the cathode is set to 0.12 and the particle is charged with C rate 100. The simulation is run until a state of charge of 0.15 is reached. In this range a phase-field transformation from bulk to separated state happens as seen in Figure 6a. The time interval T is discretized as T_τ into N_t steps of equal size τ_{Ref}. The discretized lithium ion concentration at each time t in T_τ is condensed to a solution $c_h \in (V_h \times V_h \times W_h) \times T_\tau$. Then a norm $||\cdot||$ on the discretized space-time domain $(V_h \times V_h \times W_h) \times T_\tau$ is given as

$$||c_h|| = \sqrt{\sum_{i=1}^{N_x} \sum_{j=1}^{N_y} \sum_{k=1}^{N_t} c_h(ih, jh; k\tau)^2} \tag{47}$$

A relative error measure is defined as

$$e = \frac{||c_h - c_{\text{Ref}}||}{||c_{\text{Ref}}||}, \tag{48}$$

given a reference solution c_{Ref}. As derived before, the numerical error estimate for the presented scheme is $O(h+\tau)$, where h is the mesh size and τ is the time-step size. The numerical solutions to the combinations of mesh width and time step size given in Table 4 are calculated. The solution on the finest mesh width is used as the reference solution. The coarse solutions are projected cell-wise constant into the discretized space of the reference solution. Then Figure 6b shows the plot of the error with logarithmic axes. The binary logarithm of the discrete error e is plotted against the binary logarithm of the quotient $\frac{\tau}{\tau_{\text{Ref}}} = \frac{h}{h_{\text{Ref}}}$. As the quotient $\frac{\tau}{h}$ is fixed, linear convergence is expected. The numerical convergence rate is $O((h+\tau)^{0.69})$.

4. Numerical tests

In this section the presented electrochemical model and the numerical method are applied for several simulation cases. Different microstructures of the cathode

h / nm	1	0.5	0.25	0.125	0.0625	0.03125
τ / µs	51200	25600	12800	6400	3200	1600

Table 4: Numerical convergence data, the solution on the finest grid is used as a reference solution.

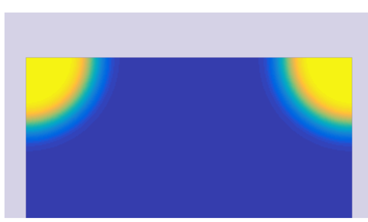

(a) The rectangular particle in a state of charge $SOC = 0.15$. The particle has separated into lithium-rich and lithium-poor phases.

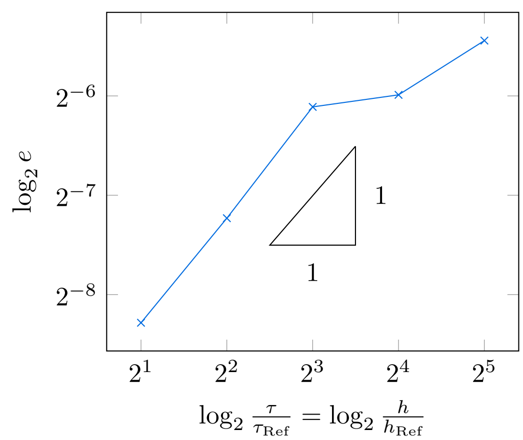

(b) Results of the numerical convergence test in a binary logarithmic plot. Depicted is the error in the lithium ion concentration (blue) and a linear slope for comparison.

Figure 6: A numerical convergence test on a rectangular particle demonstrates the numerical method.

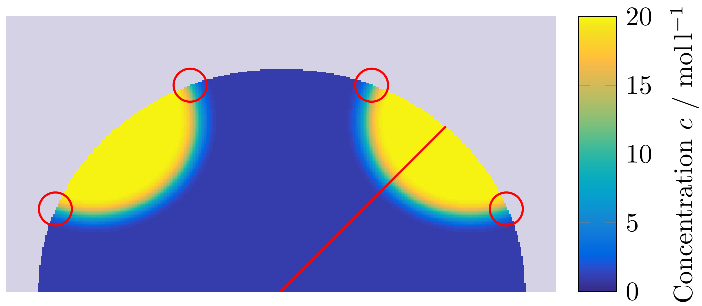

Figure 7: Spinodal decomposition in a particle shaped like a half circle. The color illustrates the distribution of lithium ions inside the circular cathode particle. The red line denotes the location that is represented in Figure 8. The red circles indicate phase interface region at the solid-electrolyte interface.

particle are simulated and the influence on the battery voltage is investigated. The phase-field method requires time steps in the range of 10 to 100 milliseconds to resolve the evolution of the phase interface along the cathode particle surface. The simulation is limited to short simulation times and high C rates between 10 and 100.

4.1. Spinodal decomposition

A domain with width and height 100 nm and a circular cathode particle as in Figure 5 is considered. The spatial discretization was chosen as $N_x = N_y = 400$. The particle is charged with C rate 100 from an initial state of charge of 0.01 to 0.25. Figure 7 shows the cathode particle at the final state of charge 0.25. Figure 8 shows the lithium ion concentration along the indicated line in Figure 7 for different states of charge.

In the beginning at a state of charge 0.05 the concentration inside the particle rises uniformly at the surface and in the center of the particle. This is called the bulk state or solid-diffusion state. The diffusivity coefficient inside the solid material is high enough in comparison to the particle radius to distribute the lithium-ion flux at the electrode-electrolyte boundary. As soon as the state of charge 0.12 (see Point S in Figure 2) is exceeded, the lithium ions inside inside the particle separate in lithium-rich and lithium-poor phases. This process is called spinodal decomposition. The exact distribution of the phases inside the particle depends on the microstructure, the C rate and the parameters used in the phase-field model. While in the bulk state the lithium ion concentration exhibits a radial symmetry inside the circular particle, in the phase-separated state this symmetry is broken in favor of two lithium-rich phases at the surface. At the state of charge 0.1225 the lithium ion concentration at the surface reaches the maximum equilibrium concentration $c = 0.987c_m$ and a lithium-rich phase is established. Finally at state of charge 0.25 the phase-separation is completed and a lithium-poor phase has emerged with the minimum equilibrium concentration $c = 0.013c_m$.

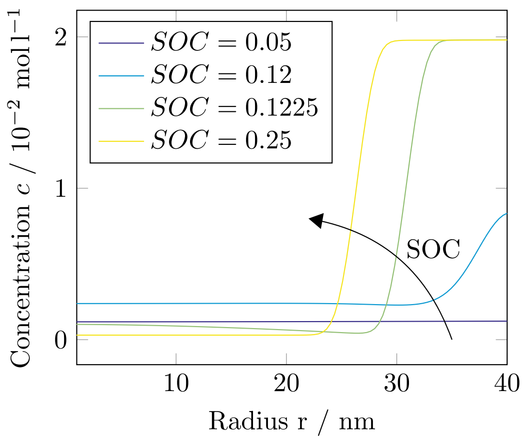

Figure 8: Concentration along the indicated line in Figure 7 for different states of charge.

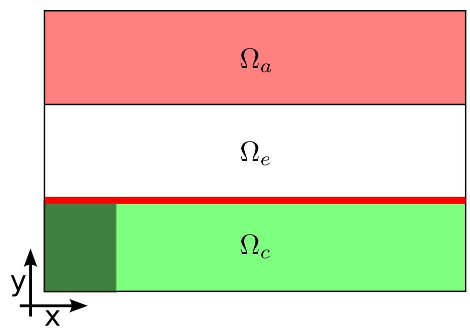

Figure 9: A flat three-layer structure used in the comparison of exchange current densities (not to scale). The left part of the cathode domain (darker green) is initialized with a lithium-rich phase that grows along the particle surface during charging.

4.2. Exchange current densities

In solid-solution theory and one-dimensional phase-field models [10] the concentration gradient in the electrode material is perpendicular to the surface. The abundance of a concentration gradient along the interface simplifies the choice of a consistent exchange current density i_0 in the Butler-Volmer equations.

In the presented model it is expected that both lithium-rich and lithium-poor phases emerge along the surface of the solid material at the same time. Hence it is also possible that a phase interface region resides along the particle surface. Figure 7 shows the phase interface region at the particle surfaces indicated by red circles.

In a first simulation this situation is enforced by the initial conditions. Different models for the exchange current density are investigated and compared.

A flat thin three-layer structure is chosen for this simulation. The simple microstructure simplifies the investigation of the influence of the exchange current

Interface width	3.3	6.7	10.0	13.3	16.7
Model A	9.44%	11.81%	16.86%	21.28%	22.74%
Model B	17.50%	22.10%	29.83%	35.76%	36.81%

Table 5: Fraction of electric current through phase interface region

density. The structure is 10 nm thick in thickness direction and 100 nm wide. The C rate 100 is applied. An asymmetrical initial lithium ion distribution in the solid phase favors the nucleation of a lithium-rich phase on the left side as seen in Figure 9. For the exchange current density, both Model A and B as introduced in Section 2, Eqs. (21), (22), are numerically simulated on a set of different phase-field interface widths L from 3.3 nm to 16.7 nm.

Figure 10 displays the particle surface current density i_{se} along the electrode-electrolyte boundary at state of charge $SOC = 0.5$. The center of the phase interface is at 50 nm and the phase interface region is present equally between the left and the right.

In the upper plot, the lithium ion concentration along the solid-electrolyte-interface is shown. The nucleation of a lithium-rich phase on the left side of the cathode is favored by a high local lithium concentration of $1.8 \cdot 10^{-2}\ \mathrm{mol\,l^{-1}}$. In the mid plot Model A (Eq. (21)) was used for the simulation. The surface current density i_{se} is large in the lithium-rich phase and rises near the phase interface region. In the lithium-poor phase it is ten times smaller than at the maximum . The integral of the surface current density over the phase interface region converges numerically to zero. In the lower plot Model B (Eq. (22)) was used for the simulation. The surface current density is distributed equally to both lithium-rich and lithium-poor phases. The peak surface current density is dependent on the interface width parameter L used in the phase-field model.

Table 5 shows the fraction of the electric current through the phase interface region for both Model A and B and different phase-field interface widths L. For both models the electric current transported through the phase interface region gets smaller for smaller interface widths. In Model B the fraction of the entire current approximately twice as high as in Model A.

4.3. Battery cell voltage

In this example the influence of charging rate on the battery cell voltage is investigated. The cell voltage is defined as the difference of the electric potential between anode and cathode. Due to high conductivity the electric potential is approximately constant inside each domain. As a first step the jump $\phi_{se,s} - \phi_{se,e}$ in the electric potential at the solid-electrolyte interfaces will be examined separately for anode and cathode. Then the cell voltage as the sum of both jumps will be discussed.

One-dimensional structure

A one-dimensional structure of thickness 100 nm built from anode (40 nm), electrolyte (20 nm) and cathode (40 nm) domain (in this order) is used to

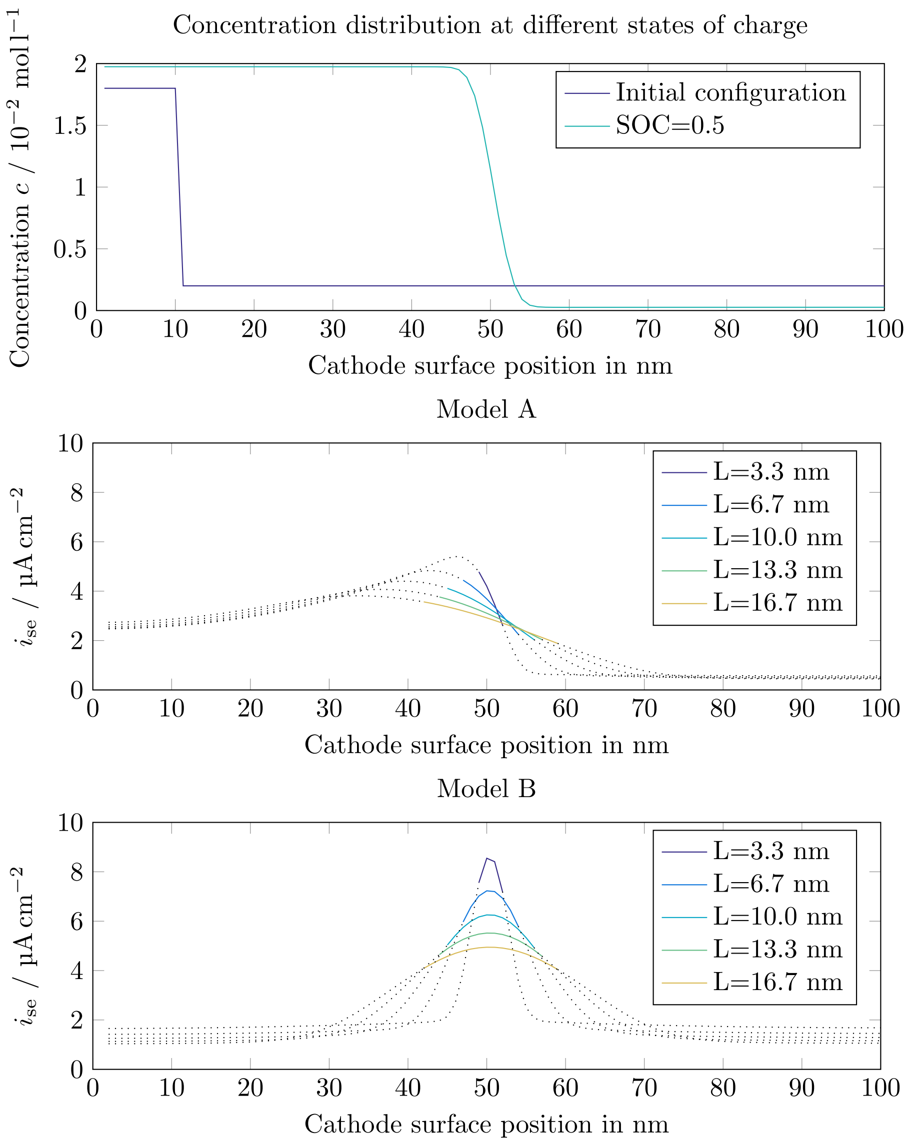

Figure 10: A comparison of two different models for the exchange current density i_0 for different interface widths L. The upper plot shows the lithium ion concentration in the initial state and for the state of charge 0.5. The mid and lower plot show the Butler-Volmer current i_{se} along the cathode surface (indicated in Figure 9 in red) for different phase-field interface widths L. Two models for the exchange current density are compared, Model A (Eq. (21)) and Model B (Eq. (22)).

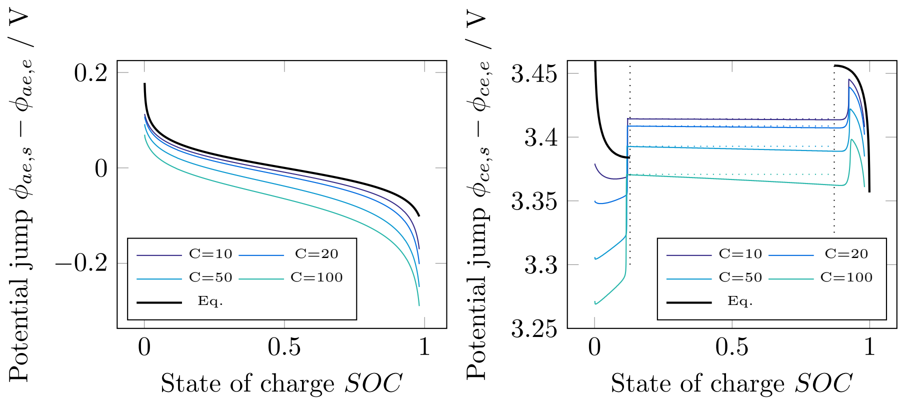

Figure 11: Voltage jump at the solid-electrolyte interface in an one-dimensional battery structure.

illustrate the basic properties of a battery cell voltage curve. Different C rates $\in \{10, 20, 50, 100\}$ are applied. The capacity of the anode is chosen to be the same as the capacity of the cathode particle.

The left plot in Figure 11 shows the potential difference between the anode domain and the electrolyte domain plotted against state of charge in the cathode. In the equilibrium the Nernst overpotential η in Eq. (23) is zero and the concentration inside the anode particle is constant due to diffusion. So the potential jump $\phi_{ae,a} - \phi_{ae,e}$ between anode and electrolyte can be expressed using the logarithmic diffusion potential $\mu_a(c)$ depending on the state of charge,

$$\begin{aligned} \eta = \phi_{ae,a} - \phi_{ae,e} - \bar{U}_a + \frac{\mu_a(c)}{F} = 0 \\ \Rightarrow \phi_{ae,a} - \phi_{ae,e} = \bar{U}_a - \frac{\mu_a(c)}{F} = \bar{U}_a - \frac{RT}{F} \log \frac{SOC}{1 - SOC}. \end{aligned} \tag{49}$$

The equilibrium solution curve resulting from this approximation is shown in the plot in bold. The voltage curves approach the analytical approximation in Eq. (49) for smaller C rates, because the Nernst overpotential gets smaller.

The right plot of Figure 11 shows the potential difference at the cathode-electrolyte interface. The vertical dotted lines show the states of charge that correspond to the concentrations of spontaneous spinodal decomposition as explained in Remark 2.

The equilibrium solution for the potential jump $\phi_{ce,c} - \phi_{ce,e}$ at the electrolyte-cathode-boundary can be derived as

$$\begin{aligned} \eta = \phi_{ce,c} - \phi_{ce,e} - \bar{U}_c + \frac{\mu_c(c)}{F} = 0 \\ \Rightarrow \phi_{ce,c} - \phi_{ce,e} = \bar{U}_c - \frac{\mu_c(c)}{F}. \end{aligned} \tag{50}$$

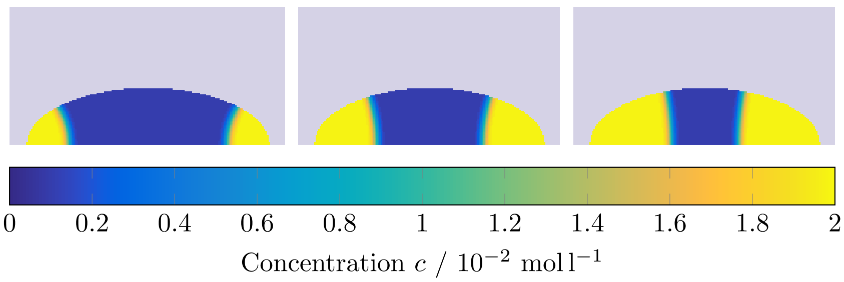

Figure 12: An ellipsoidal particle for states of charge 0.2, 0.4 and 0.6.

At the critical state of charge 0.12 (see Figure 2) the lithium ions separate in lithium-rich and lithium-poor phases as shown in Subsection 4.1. Given the Maxwell construction and the higher equilibrium concentration $c_2 \approx 0.987c_m$ the resulting plateau electric potential can be calculated. The interface condition in Eq. (20) is solved for the potential jump $\phi_{ce,c} - \phi_{ce,e}$ at the electrolyte-cathode-boundary. The chemical potential $\mu_c(c)$ inside the solid at the particle surface is zero in a phase-separated state.

$$\phi_{ce,c} - \phi_{ce,e} = \bar{U}_c - 2\frac{RT}{F} \operatorname{arcsinh}\left(\frac{i_{\mathrm{se}}}{2k\sqrt{c_{e,0}c_2\frac{c_m}{2}}} \right). \tag{51}$$

The particle surface current i_{se} is calculated dependent on the C rate. The resulting plateau electric potentials are indicated by horizontal black lines in Figure 11.

For high C rates now the particle surface concentration rises even further which decreases the electric potential, while for small C rates the diffusivity prevails and the voltage stays constant. These approximations to the cell voltage are given by horizontal dotted lines in the color corresponding to the C rate. The phase separation ends after the state of charge corresponding to the reverse spinodal decomposition point and the concentration decreases in the particle as the lithium ion concentration is distributed evenly in the particle. Therefore the voltage rises again and the equilibrium solution in Eq. (50) is valid again.

With this understanding it is now possible to take a look at a complex two-dimensional example and to distinguish between already established effects and new effects that arise from the structure.

Two-dimensional structure

Figure 5 introduces structures of different ellipsoidal particles. An analytical dimensionless description of the cathode domain Ω_c inside a square domain Ω is given as

$$\Omega_c = \left\{ (x, y) \in \Omega \,\middle|\, \frac{(x - x_0)^2}{a^2} + \frac{(y - y_0)^2}{b^2} < r^2 \right\}, \tag{52}$$

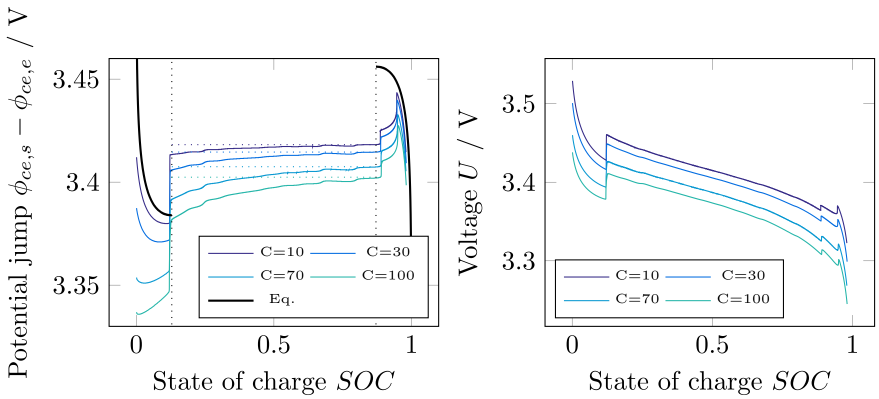

Figure 13: Voltage jump at the cathode electrolyte interface in a two-dimensional ellipsoidal battery structure and the resulting battery cell voltage.

where y is the thickness direction. The values $a = 100$ nm and $b = 50$ nm are used to describe a flat ellipsoidal particle with radius $r_0 = 40$ nm around the center $(x_0, y_0) = (50\text{ nm}, 0\text{ nm})$. A microstructure with width and height 100 nm is considered and the C rate 100 is applied. The capacity of the anode is then chosen to be the same as the capacity of the cathode particle.

The electric potential jump at the anode-electrolyte interface is similar to the one given in Figure 11 and is therefore omitted.

The left plot in Figure 13 shows the potential differences between the cathode domain and the electrolyte domain plotted against state of charge in the cathode. The same annotations as in the right plot in Figure 11 have been added. While in the one-dimensional case, the potential difference decreased for an increasing state of charge in the interval $SOC \in [0.13, 0.9]$, here the potential difference rises. In the one-dimensional case, the particle surface concentration rose as the state of charge increased. However, as shown before in Subsection 4.2, the major particle surface concentration flow is applied near the phase interface. There the lithium-rich phase is able to grow while still retaining the equilibrium lithium ion concentration c_2.

Finally, the right plot in Figure 13 shows the resulting battery cell voltage as the sum of both voltage jumps at the solid-electrolyte interfaces. Overall the voltage drop at the anode-electrolyte interface prevails and the effects of phase transitions can only be recognized as small discontinuities in the voltage curve.

4.4. Variation of cathode particle size and shape

In this section, the effect of cathode particle size and particle shape on the charging behavior is examined. For transport problems, the ratio between the size of the interface region Γ_{ce} and the volume of the intercalated domain Ω_c is important. Also the shape of the domain affects diffusive processes. Furthermore, each phase-field model involves an intrinsic length scale and therefore the

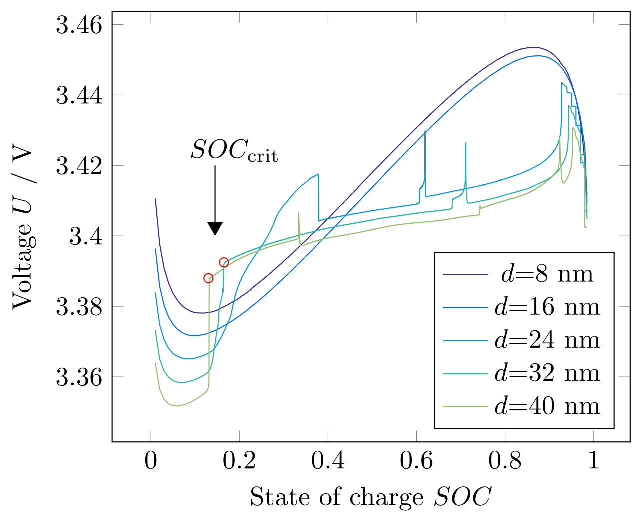

Figure 14: Voltage curves for different particle sizes. Critical states of charge are indicated with red circles for larger particle sizes.

ratio between the size of the cathode domain Ω_c and the phase-field interface length L is relevant to the solution.

Size effects

A spherical cathode particle as introduced in Figure 5 with varying size is charged from an empty state of charge $SOC = 0.01$ with C rate 100. The particle diameter is varied from 8 nm to 40 nm and embedded in a corresponding domain with width and height varying from 10 nm to 50 nm. The spatial discretization is set to $N_x = N_y = 200$.

Figure 14 shows different voltage curves depending on the diameter size of a spherical particle. For larger particle sizes with particle diameter $d \in \{24\text{ nm}; 32\text{ nm}; 40\text{ nm}\}$ the charging of the particle progresses as shown before in Subsection 4.1 with the emerging of a lithium-rich phase, the growth of this phase and the reversal of the phase separation. The voltage discontinuity indicates the critical state of charge for which a phase separation happens. This critical state of charge is dependent on the particle diameter and it gets larger for smaller particle sizes. The smooth voltage curves for particle sizes $d \in \{8\text{ nm}; 16\text{ nm}\}$ show that the lithium ions do not separate into lithium-rich and poor phases. The interface width L separating both phases is large in comparison to the particle diameter and the particle stays in the bulk state for the charging process.

Shape effects

In another example the effect of the particle shape on the process of phase separation is investigated. In a domain with width and height 100 nm and C

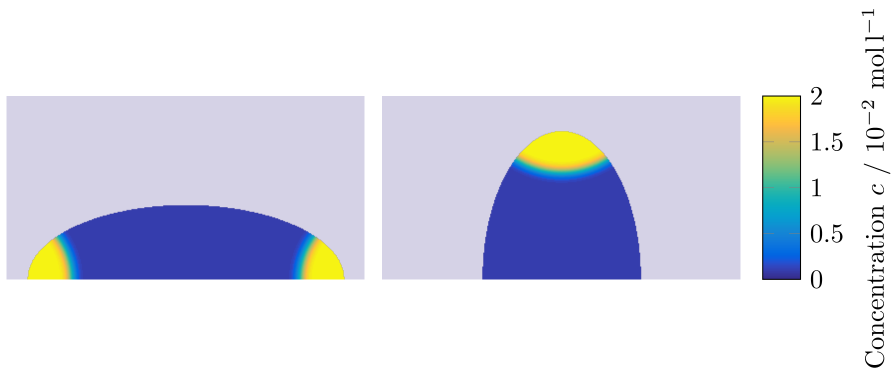

Figure 15: Ellipsoidal particles at SOC=0.14

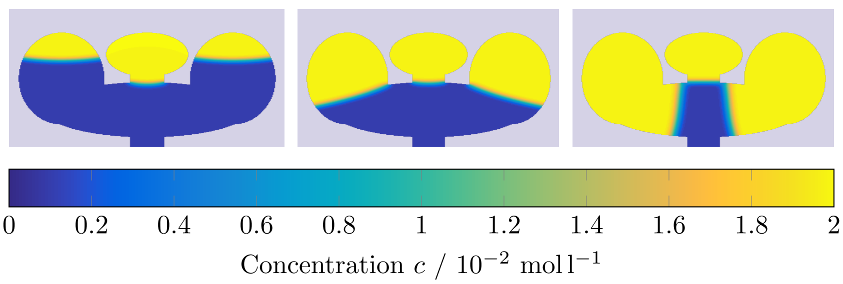

Figure 16: The structure being charged at SOC=0.28,0.56,0.83

rate 100 two different ellipsoidal particles are charged. The spatial discretization is set to $N_x = N_y = 400$. Figure 15 shows both particles at the state of charge $SOC = 0.14$ in a phase-separated stage.

The occurrence of the lithium-rich phases can be explained. Starting at the bulk phase, the particle surface current i_{se} is constant along the particle surface. At areas of the particle structure with high local boundary curvature, the concentration rises faster than along flat edges. Therefore a small concentration gradient is built up inside the particle that later results in the formation of a lithium-rich phase in corners.

The curved phase interface separating lithium-rich and poor phases has minimum area under the constraint to contain the lithium-rich phase. The energy related to the Laplacian in the free energy functional in Eq. (13) is minimal, comparable to the effect of surface tension. Due to Eq. (32) the phase interface is always perpendicular to the particle surface.

4.5. Simulation of a complex microstructure

In a final example a complex microstructure built from geometric shapes is charged. A domain with width and height 100 nm and C rate 100 is used. The spatial discretization is set to $N_x = N_y = 400$. Figure 16 shows the numerical solution of the lithium ion concentration in the cathode material during different states of charge.

It can be seen that the different lithium-rich phases evolve with different rates. An important factor is the evolution of the phase interface. As explained before, growth of this area involves increasing the internal energy. Therefore the surface current and the diffusion inside the particle evolve such that some lithium-rich regions are preferred for growth. At state of charge $SOC = 0.69$ the area for the phase interface of the mid lithium-rich phase is small and potential growth involves growth of its phase interface area, whereas the other two lithium-rich phases are able to grow without enlarging the area of the phase interface.

5. Summary and conclusions

An electrochemical model implementing the transport of lithium ions inside a battery cell and the transmission in the solid-electrolyte interface is introduced in Section 2. While previous theory is limited to a diffusion model, the model is extended to include arbitrary electrochemical potentials. A phase-field potential is presented and applied inside the cathode material to model the separation into lithium-poor and lithium-rich phases.

Remark 2 analyzes the phase-field potential and gives an estimate for the interface width of 3.3 nm. Therefore a fine spatial discretization of 1 nm is required which allows for simulation domains of width and height 200 nm on a regular mesh. As time steps have to stay below 100 milliseconds to resolve the evolution of the phase interface, computational costs limit the simulation to higher C rates in the range of 10 to 100.

The finite volume method presented in Section 3 is suitable for transmission problems with jump conditions on interfaces inside the domain as well as phase-field models. It allows for the resolution of different solid microstructures. The regular mesh enables the use of accelerated numerical methods such as Fourier methods for parabolic equations. The method shows numerical convergence on a finer discretization.

Between states of charge 0.13 and 0.9, the cathode material undergoes phase separation into lithium-poor and lithium-rich phases, a process called spinodal decomposition in Subsection 4.1. Both phases are present at the particle surface. By this, the model of the exchange current density has an influence on the distribution of the solid-electrolyte current along the particle surface as shown in Subsection 4.2.

The electric potential difference at the cathode-electrolyte interface approaches the equilibrium solution for smaller C rates. It is non-smooth as the phase separation begins at state of charge 0.13. The resulting plateau voltage is calculated depending on the C rate in Subsection 4.3.

Size and shape of the cathode microstructure affect the emergence of lithium-rich phases. Smaller particles do not provide enough inner volume for the development a phase interface and phase separation is suppressed. Peaks in the surface boundary eventuate in high local lithium ion concentrations (Subsection 4.4).

Finally, the microstructure in Subsection 4.5 reveals the complex diffusion processes inside electrode material. The interface area between the phases is minimized and its shape depends on the microstructure. The lithium ions are transferred inside the particle between different lithium-rich phases by diffusion.

Future work includes the extension of the electrochemical mode to include three-dimensional structures and linear elasticity. The computational costs can be significantly reduced by the application of fast Fourier methods for the spatial differentiation on regular voxel meshes instead of finite differences. Numerical simulations including inter-particle diffusion on the microscale give further insight into the aging processes resulting in capacity loss and battery failing.

Acknowledgment Prof. Arnulf Latz is thanked for fruitful discussion on the Butler-Volmer solid-electrolyte interface conditions. Furthermore for the support in the modeling of exchange current densities and the interpretation of electric potential differences resulting from a phase-separated cathode particle.

References

[1] Christer Andersson. *Phase-field Simulation of Dendritic Solidification*. PhD thesis, Royal Institute of Technology Stockholm, 2002.

[2] Martin Z Bazant. Theory of Chemical Kinetics and Charge Transfer based on Nonequilibrium Thermodynamics. *Accounts of chemical research*, 46(5):1144–1160, 2013.

[3] M. Broussely, Ph. Biensan, F. Bonhomme, Ph. Blanchard, S. Herreyre, K. Nechev, and R.J. Staniewicz. Main aging mechanisms in Li ion batteries. *Journal of Power Sources*, 146(1-2):90–96, 2005.

[4] John Cahn and John Hilliard. Free Energy of a Nonuniform System. I. Interfacial Free Energy. *The Journal of Chemical Physics*, 28(1958):258–267, 1958.

[5] Di Chen, Sylvio Indris, Michael Schulz, Benedikt Gamer, and Reiner Mönig. In situ scanning electron microscopy on lithium-ion battery electrodes using an ionic liquid. *Journal of Power Sources*, 196(15):6382–6387, 2011.

[6] Zungsun Choi, Dominik Kramer, and Reiner Mönig. Correlation of stress and structural evolution in Li4Ti5O12-based electrodes for lithium ion batteries. *Journal of Power Sources*, 240:245–251, 2013.

[7] Daniel a Cogswell and Martin Z Bazant. Coherency strain and the kinetics of phase separation in LiFePO4 nanoparticles. *ACS nano*, 6(3):2215–25, 2012.

[8] M. A. Crisfield. An arc-length method including line searches and accelerations. *International Journal for Numerical Methods in Engineering*, 19(9):1269–1289, 1983.

[9] S. Dargaville and T. W. Farrell. The persistence of phase-separation in LiFePO4 with two-dimensional Li+ transport: The Cahn-Hilliard-reaction equation and the role of defects. *Electrochimica Acta*, 94:143–158, 2013.

[10] Wolfgang Dreyer, Clemens Guhlke, and Rüdiger Müller. Rational modeling of electrochemical double-layers and derivation of Butler-Volmer equations. *WIAS Preprint*, (1860), 2013.

[11] M. Ebner, F. Marone, M. Stampanoni, and V. Wood. Visualization and Quantification of Electrochemical and Mechanical Degradation in Li Ion Batteries. *Science*, 342(6159):716–720, 2013.

[12] Lawrence Evans. *Partial Differential Equations.* American Mathematical Society, 1996.

[13] David Eyre. Unconditionally Gradient Stable Time Marching the Cahn-Hilliard Equation. *MRS Proceedings*, 529, 1998.

[14] Isaac Harari and John Dolbow. Analysis of an efficient finite element method for embedded interface problems. *Computational Mechanics*, 46:205–211, 2010.

[15] Magalie Huttin. Phase-field modeling of the infuence of mechanical stresses on charging and discharging processes in lithium ion batteries. 2014.

[16] A. Latz and J. Zausch. Thermodynamic consistent transport theory of Li-ion batteries. *Journal of Power Sources*, 196(6):3296–3302, 2011.

[17] Arnulf Latz and Jochen Zausch. Thermodynamic derivation of a Butler-Volmer model for intercalation in Li-ion batteries. *Electrochimica Acta*, 110:358–362, 2013.

[18] Claudio Mattiussi. An Analysis of Finite Volume, Finite Element, and Finite Difference Methods Using Some Concepts from Algebraic Topology. *Journal of Computational Physics*, 133(2):289–309, 1997.

[19] S.L. Mitchell and M. Vynnycky. Finite-difference methods with increased accuracy and correct initialization for one-dimensional Stefan problems. *Applied Mathematics and Computation*, 215(4):1609–1621, 2009.

[20] John Newman and Karen Thomas-Alyea. *Electrochemical Systems.* John Wiley & Sons, 2004.

[21] J Nocedal and S J Wright. *Numerical Optimization.* Springer-Verlag New York, 1999.

[22] Peter Popov and Svetozar Margenov. Microscale Modelling of Li-ion batteries. *Berichte des Fraunhofer ITWM*, (191), 2010.

[23] Nikolas Provatas and Ken Elder. *Phase-Field Methods in Materials Science and Engineering*. Wiley-VCH, 2010.

[24] David Schrade. *Microstructural modeling of ferroelectric material behavior*. PhD thesis, TU Kaiserslautern, 2010.

[25] Maxim Taralov. *Simulation of Degradation Processes in Lithium-Ion Batteries*. PhD thesis, TU Kaiserslautern, 2015.

[26] Y. Zeng, P. Albertus, R. Klein, N. Chaturvedi, A. Kojic, M. Z. Bazant, and J. Christensen. Efficient Conservative Numerical Schemes for 1D Nonlinear Spherical Diffusion Equations with Applications in Battery Modeling. *Journal of the Electrochemical Society*, 160(9):A1565–A1571, 2013.

[27] Yi Zeng and Martin Z Bazant. Phase separation dynamics in isotropic Ion-intercalation particles. 74(4):980–1004, 2014.

[28] Yujie Zhu, Jiang Wei Wang, Yang Liu, Xiaohua Liu, Akihiro Kushima, Yihang Liu, Yunhua Xu, Scott X. Mao, Ju Li, Chunsheng Wang, and Jian Yu Huang. In Situ Atomic-Scale Imaging of Phase Boundary Migration in FePO4 Microparticles During Electrochemical Lithiation. *Advanced Materials*, 25(c):5461–5466, 2013.

Published reports of the Fraunhofer ITWM

The PDF-files of the following reports are available under:
www.itwm.fraunhofer.de/presse-und-publikationen/

1. D. Hietel, K. Steiner, J. Struckmeier
A Finite - Volume Particle Method for Compressible Flows
(19 pages, 1998)

2. M. Feldmann, S. Seibold
Damage Diagnosis of Rotors: Application of Hilbert Transform and Multi-Hypothesis Testing
Keywords: Hilbert transform, damage diagnosis, Kalman filtering, non-linear dynamics
(23 pages, 1998)

3. Y. Ben-Haim, S. Seibold
Robust Reliability of Diagnostic Multi-Hypothesis Algorithms: Application to Rotating Machinery
Keywords: Robust reliability, convex models, Kalman filtering, multi-hypothesis diagnosis, rotating machinery, crack diagnosis
(24 pages, 1998)

4. F.-Th. Lentes, N. Siedow
Three-dimensional Radiative Heat Transfer in Glass Cooling Processes
(23 pages, 1998)

5. A. Klar, R. Wegener
A hierarchy of models for multilane vehicular traffic
Part I: Modeling
(23 pages, 1998)

Part II: Numerical and stochastic investigations
(17 pages, 1998)

6. A. Klar, N. Siedow
Boundary Layers and Domain Decomposition for Radiative Heat Transfer and Diffusion Equations: Applications to Glass Manufacturing Processes
(24 pages, 1998)

7. I. Choquet
Heterogeneous catalysis modelling and numerical simulation in rarified gas flows Part I: Coverage locally at equilibrium
(24 pages, 1998)

8. J. Ohser, B. Steinbach, C. Lang
Efficient Texture Analysis of Binary Images
(17 pages, 1998)

9. J. Orlik
Homogenization for viscoelasticity of the integral type with aging and shrinkage
(20 pages, 1998)

10. J. Mohring
Helmholtz Resonators with Large Aperture
(21 pages, 1998)

11. H. W. Hamacher, A. Schöbel
On Center Cycles in Grid Graphs
(15 pages, 1998)

12. H. W. Hamacher, K.-H. Küfer
Inverse radiation therapy planning - a multiple objective optimisation approach
(14 pages, 1999)

13. C. Lang, J. Ohser, R. Hilfer
On the Analysis of Spatial Binary Images
(20 pages, 1999)

14. M. Junk
On the Construction of Discrete Equilibrium Distributions for Kinetic Schemes
(24 pages, 1999)

15. M. Junk, S. V. Raghurame Rao
A new discrete velocity method for Navier-Stokes equations
(20 pages, 1999)

16. H. Neunzert
Mathematics as a Key to Key Technologies
(39 pages, 1999)

17. J. Ohser, K. Sandau
Considerations about the Estimation of the Size Distribution in Wicksell's Corpuscle Problem
(18 pages, 1999)

18. E. Carrizosa, H. W. Hamacher, R. Klein, S. Nickel
Solving nonconvex planar location problems by finite dominating sets
Keywords: Continuous Location, Polyhedral Gauges, Finite Dominating Sets, Approximation, Sandwich Algorithm, Greedy Algorithm
(19 pages, 2000)

19. A. Becker
A Review on Image Distortion Measures
Keywords: Distortion measure, human visual system
(26 pages, 2000)

20. H. W. Hamacher, M. Labbé, S. Nickel, T. Sonneborn
Polyhedral Properties of the Uncapacitated Multiple Allocation Hub Location Problem
Keywords: integer programming, hub location, facility location, valid inequalities, facets, branch and cut
(21 pages, 2000)

21. H. W. Hamacher, A. Schöbel
Design of Zone Tariff Systems in Public Transportation
(30 pages, 2001)

22. D. Hietel, M. Junk, R. Keck, D. Teleaga
The Finite-Volume-Particle Method for Conservation Laws
(16 pages, 2001)

23. T. Bender, H. Hennes, J. Kalcsics, M. T. Melo, S. Nickel
Location Software and Interface with GIS and Supply Chain Management
Keywords: facility location, software development, geographical information systems, supply chain management
(48 pages, 2001)

24. H. W. Hamacher, S. A. Tjandra
Mathematical Modelling of Evacuation Problems: A State of Art
(44 pages, 2001)

25. J. Kuhnert, S. Tiwari
Grid free method for solving the Poisson equation
Keywords: Poisson equation, Least squares method, Grid free method
(19 pages, 2001)

26. T. Götz, H. Rave, D. Reinel-Bitzer, K. Steiner, H. Tiemeier
Simulation of the fiber spinning process
Keywords: Melt spinning, fiber model, Lattice Boltzmann, CFD
(19 pages, 2001)

27. A. Zemitis
On interaction of a liquid film with an obstacle
Keywords: impinging jets, liquid film, models, numerical solution, shape
(22 pages, 2001)

28. I. Ginzburg, K. Steiner
Free surface lattice-Boltzmann method to model the filling of expanding cavities by Bingham Fluids
Keywords: Generalized LBE, free-surface phenomena, interface boundary conditions, filling processes, Bingham viscoplastic model, regularized models
(22 pages, 2001)

29. H. Neunzert
»Denn nichts ist für den Menschen als Menschen etwas wert, was er nicht mit Leidenschaft tun kann«
Vortrag anlässlich der Verleihung des Akademiepreises des Landes Rheinland-Pfalz am 21.11.2001
Keywords: Lehre, Forschung, angewandte Mathematik, Mehrskalenanalyse, Strömungsmechanik
(18 pages, 2001)

30. J. Kuhnert, S. Tiwari
Finite pointset method based on the projection method for simulations of the incompressible Navier-Stokes equations
Keywords: Incompressible Navier-Stokes equations, Meshfree method, Projection method, Particle scheme, Least squares approximation
AMS subject classification: 76D05, 76M28
(25 pages, 2001)

31. R. Korn, M. Krekel
Optimal Portfolios with Fixed Consumption or Income Streams
Keywords: Portfolio optimisation, stochastic control, HJB equation, discretisation of control problems
(23 pages, 2002)

32. M. Krekel
Optimal portfolios with a loan dependent credit spread
Keywords: Portfolio optimisation, stochastic control, HJB equation, credit spread, log utility, power utility, non-linear wealth dynamics
(25 pages, 2002)

33. J. Ohser, W. Nagel, K. Schladitz
The Euler number of discretized sets – on the choice of adjacency in homogeneous lattices
Keywords: image analysis, Euler number, neighborhod relationships, cuboidal lattice
(32 pages, 2002)

34. I. Ginzburg, K. Steiner
Lattice Boltzmann Model for Free-Surface flow and Its Application to Filling Process in Casting
Keywords: Lattice Boltzmann models; free-surface phenomena; interface boundary conditions; filling processes; injection molding; volume of fluid method; interface boundary conditions; advection-schemes; upwind-schemes
(54 pages, 2002)

35. M. Günther, A. Klar, T. Materne, R. Wegener
Multivalued fundamental diagrams and stop and go waves for continuum traffic equations
Keywords: traffic flow, macroscopic equations, kinetic derivation, multivalued fundamental diagram, stop and go waves, phase transitions
(25 pages, 2002)

36. S. Feldmann, P. Lang, D. Prätzel-Wolters
Parameter influence on the zeros of network determinants
Keywords: Networks, Equicofactor matrix polynomials, Realization theory, Matrix perturbation theory
(30 pages, 2002)

37. K. Koch, J. Ohser, K. Schladitz
Spectral theory for random closed sets and estimating the covariance via frequency space
Keywords: Random set, Bartlett spectrum, fast Fourier transform, power spectrum
(28 pages, 2002)

38. D. d'Humières, I. Ginzburg
Multi-reflection boundary conditions for lattice Boltzmann models
Keywords: lattice Boltzmann equation, boudary condistions, bounce-back rule, Navier-Stokes equation
(72 pages, 2002)

39. R. Korn
Elementare Finanzmathematik
Keywords: Finanzmathematik, Aktien, Optionen, Portfolio-Optimierung, Börse, Lehrerweiterbildung, Mathematikunterricht
(98 pages, 2002)

40. J. Kallrath, M. C. Müller, S. Nickel
Batch Presorting Problems: Models and Complexity Results
Keywords: Complexity theory, Integer programming, Assigment, Logistics
(19 pages, 2002)

41. J. Linn
On the frame-invariant description of the phase space of the Folgar-Tucker equation
Key words: fiber orientation, Folgar-Tucker equation, injection molding
(5 pages, 2003)

42. T. Hanne, S. Nickel
A Multi-Objective Evolutionary Algorithm for Scheduling and Inspection Planning in Software Development Projects
Key words: multiple objective programming, project management and scheduling, software development, evolutionary algorithms, efficient set
(29 pages, 2003)

43. T. Bortfeld , K.-H. Küfer, M. Monz, A. Scherrer, C. Thieke, H. Trinkaus
Intensity-Modulated Radiotherapy - A Large Scale Multi-Criteria Programming Problem
Keywords: multiple criteria optimization, representative systems of Pareto solutions, adaptive triangulation, clustering and disaggregation techniques, visualization of Pareto solutions, medical physics, external beam radiotherapy planning, intensity modulated radiotherapy
(31 pages, 2003)

44. T. Halfmann, T. Wichmann
Overview of Symbolic Methods in Industrial Analog Circuit Design
Keywords: CAD, automated analog circuit design, symbolic analysis, computer algebra, behavioral modeling, system simulation, circuit sizing, macro modeling, differential-algebraic equations, index
(17 pages, 2003)

45. S. E. Mikhailov, J. Orlik
Asymptotic Homogenisation in Strength and Fatigue Durability Analysis of Composites
Keywords: multiscale structures, asymptotic homogenization, strength, fatigue, singularity, non-local conditions
(14 pages, 2003)

46. P. Domínguez-Marín, P. Hansen, N. Mladenovic , S. Nickel
Heuristic Procedures for Solving the Discrete Ordered Median Problem
Keywords: genetic algorithms, variable neighborhood search, discrete facility location
(31 pages, 2003)

47. N. Boland, P. Domínguez-Marín, S. Nickel, J. Puerto
Exact Procedures for Solving the Discrete Ordered Median Problem
Keywords: discrete location, Integer programming
(41 pages, 2003)

48. S. Feldmann, P. Lang
Padé-like reduction of stable discrete linear systems preserving their stability
Keywords: Discrete linear systems, model reduction, stability, Hankel matrix, Stein equation
(16 pages, 2003)

49. J. Kallrath, S. Nickel
A Polynomial Case of the Batch Presorting Problem
Keywords: batch presorting problem, online optimization, competetive analysis, polynomial algorithms, logistics
(17 pages, 2003)

50. T. Hanne, H. L. Trinkaus
knowCube for MCDM – Visual and Interactive Support for Multicriteria Decision Making
Key words: Multicriteria decision making, knowledge management, decision support systems, visual interfaces, interactive navigation, real-life applications.
(26 pages, 2003)

51. O. Iliev, V. Laptev
On Numerical Simulation of Flow Through Oil Filters
Keywords: oil filters, coupled flow in plain and porous media, Navier-Stokes, Brinkman, numerical simulation
(8 pages, 2003)

52. W. Dörfler, O. Iliev, D. Stoyanov, D. Vassileva
On a Multigrid Adaptive Refinement Solver for Saturated Non-Newtonian Flow in Porous Media
Keywords: Nonlinear multigrid, adaptive refinement, non-Newtonian flow in porous media
(17 pages, 2003)

53. S. Kruse
On the Pricing of Forward Starting Options under Stochastic Volatility
Keywords: Option pricing, forward starting options, Heston model, stochastic volatility, cliquet options
(11 pages, 2003)

54. O. Iliev, D. Stoyanov
Multigrid – adaptive local refinement solver for incompressible flows
Keywords: Navier-Stokes equations, incompressible flow, projection-type splitting, SIMPLE, multigrid methods, adaptive local refinement, lid-driven flow in a cavity
(37 pages, 2003)

55. V. Starikovicius
The multiphase flow and heat transfer in porous media
Keywords: Two-phase flow in porous media, various formulations, global pressure, multiphase mixture model, numerical simulation
(30 pages, 2003)

56. P. Lang, A. Sarishvili, A. Wirsen
Blocked neural networks for knowledge extraction in the software development process
Keywords: Blocked Neural Networks, Nonlinear Regression, Knowledge Extraction, Code Inspection
(21 pages, 2003)

57. H. Knaf, P. Lang, S. Zeiser
Diagnosis aiding in Regulation Thermography using Fuzzy Logic
Keywords: fuzzy logic,knowledge representation, expert system
(22 pages, 2003)

58. M. T. Melo, S. Nickel, F. Saldanha da Gama
Largescale models for dynamic multicommodity capacitated facility location
Keywords: supply chain management, strategic planning, dynamic location, modeling
(40 pages, 2003)

59. J. Orlik
Homogenization for contact problems with periodically rough surfaces
Keywords: asymptotic homogenization, contact problems
(28 pages, 2004)

60. A. Scherrer, K.-H. Küfer, M. Monz, F. Alonso, T. Bortfeld
IMRT planning on adaptive volume structures – a significant advance of computational complexity
Keywords: Intensity-modulated radiation therapy (IMRT), inverse treatment planning, adaptive volume structures, hierarchical clustering, local refinement, adaptive clustering, convex programming, mesh generation, multi-grid methods
(24 pages, 2004)

61. D. Kehrwald
Parallel lattice Boltzmann simulation of complex flows
Keywords: Lattice Boltzmann methods, parallel computing, microstructure simulation, virtual material design, pseudo-plastic fluids, liquid composite moulding
(12 pages, 2004)

62. O. Iliev, J. Linn, M. Moog, D. Niedziela, V. Starikovicius
On the Performance of Certain Iterative Solvers for Coupled Systems Arising in Dis-

cretization of Non-Newtonian Flow Equations
Keywords: Performance of iterative solvers, Preconditioners, Non-Newtonian flow
(17 pages, 2004)

63. R. Ciegis, O. Iliev, S. Rief, K. Steiner
On Modelling and Simulation of Different Regimes for Liquid Polymer Moulding
Keywords: Liquid Polymer Moulding, Modelling, Simulation, Infiltration, Front Propagation, non-Newtonian flow in porous media
(43 pages, 2004)

64. T. Hanne, H. Neu
Simulating Human Resources in Software Development Processes
Keywords: Human resource modeling, software process, productivity, human factors, learning curve
(14 pages, 2004)

65. O. Iliev, A. Mikelic, P. Popov
Fluid structure interaction problems in deformable porous media: Toward permeability of deformable porous media
Keywords: fluid-structure interaction, deformable porous media, upscaling, linear elasticity, stokes, finite elements
(28 pages, 2004)

66. F. Gaspar, O. Iliev, F. Lisbona, A. Naumovich, P. Vabishchevich
On numerical solution of 1-D poroelasticity equations in a multilayered domain
Keywords: poroelasticity, multilayered material, finite volume discretization, MAC type grid
(41 pages, 2004)

67. J. Ohser, K. Schladitz, K. Koch, M. Nöthe
Diffraction by image processing and its application in materials science
Keywords: porous microstructure, image analysis, random set, fast Fourier transform, power spectrum, Bartlett spectrum
(13 pages, 2004)

68. H. Neunzert
Mathematics as a Technology: Challenges for the next 10 Years
Keywords: applied mathematics, technology, modelling, simulation, visualization, optimization, glass processing, spinning processes, fiber-fluid interaction, trubulence effects, topological optimization, multicriteria optimization, Uncertainty and Risk, financial mathematics, Malliavin calculus, Monte-Carlo methods, virtual material design, filtration, bio-informatics, system biology
(29 pages, 2004)

69. R. Ewing, O. Iliev, R. Lazarov, A. Naumovich
On convergence of certain finite difference discretizations for 1D poroelasticity interface problems
Keywords: poroelasticity, multilayered material, finite volume discretizations, MAC type grid, error estimates
(26 pages,2004)

70. W. Dörfler, O. Iliev, D. Stoyanov, D. Vassileva
On Efficient Simulation of Non-Newtonian Flow in Saturated Porous Media with a Multigrid Adaptive Refinement Solver
Keywords: Nonlinear multigrid, adaptive renement, non-Newtonian in porous media
(25 pages, 2004)

71. J. Kalcsics, S. Nickel, M. Schröder
Towards a Unified Territory Design Approach – Applications, Algorithms and GIS Integration
Keywords: territory desgin, political districting, sales territory alignment, optimization algorithms, Geographical Information Systems
(40 pages, 2005)

72. K. Schladitz, S. Peters, D. Reinel-Bitzer, A. Wiegmann, J. Ohser
Design of acoustic trim based on geometric modeling and flow simulation for non-woven
Keywords: random system of fibers, Poisson line process, flow resistivity, acoustic absorption, Lattice-Boltzmann method, non-woven
(21 pages, 2005)

73. V. Rutka, A. Wiegmann
Explicit Jump Immersed Interface Method for virtual material design of the effective elastic moduli of composite materials
Keywords: virtual material design, explicit jump immersed interface method, effective elastic moduli, composite materials
(22 pages, 2005)

74. T. Hanne
Eine Übersicht zum Scheduling von Baustellen
Keywords: Projektplanung, Scheduling, Bauplanung, Bauindustrie
(32 pages, 2005)

75. J. Linn
The Folgar-Tucker Model as a Differetial Algebraic System for Fiber Orientation Calculation
Keywords: fiber orientation, Folgar–Tucker model, invariants, algebraic constraints, phase space, trace stability
(15 pages, 2005)

76. M. Speckert, K. Dreßler, H. Mauch, A. Lion, G. J. Wierda
Simulation eines neuartigen Prüfsystems für Achserprobungen durch MKS-Modellierung einschließlich Regelung
Keywords: virtual test rig, suspension testing, multibody simulation, modeling hexapod test rig, optimization of test rig configuration
(20 pages, 2005)

77. K.-H. Küfer, M. Monz, A. Scherrer, P. Süss, F. Alonso, A. S. A. Sultan, Th. Bortfeld, D. Craft, Chr. Thieke
Multicriteria optimization in intensity modulated radiotherapy planning
Keywords: multicriteria optimization, extreme solutions, real-time decision making, adaptive approximation schemes, clustering methods, IMRT planning, reverse engineering
(51 pages, 2005)

78. S. Amstutz, H. Andrä
A new algorithm for topology optimization using a level-set method
Keywords: shape optimization, topology optimization, topological sensitivity, level-set
(22 pages, 2005)

79. N. Ettrich
Generation of surface elevation models for urban drainage simulation
Keywords: Flooding, simulation, urban elevation models, laser scanning
(22 pages, 2005)

80. H. Andrä, J. Linn, I. Matei, I. Shklyar, K. Steiner, E. Teichmann
OPTCAST – Entwicklung adäquater Strukturoptimierungsverfahren für Gießereien Technischer Bericht (KURZFASSUNG)
Keywords: Topologieoptimierung, Level-Set-Methode, Gießprozesssimulation, Gießtechnische Restriktionen, CAE-Kette zur Strukturoptimierung
(77 pages, 2005)

81. N. Marheineke, R. Wegener
Fiber Dynamics in Turbulent Flows
Part I: General Modeling Framework
Keywords: fiber-fluid interaction; Cosserat rod; turbulence modeling; Kolmogorov's energy spectrum; double-velocity correlations; differentiable Gaussian fields
(20 pages, 2005)

Part II: Specific Taylor Drag
Keywords: flexible fibers; k-ε turbulence model; fiber-turbulence interaction scales; air drag; random Gaussian aerodynamic force; white noise; stochastic differential equations; ARMA process
(18 pages, 2005)

82. C. H. Lampert, O. Wirjadi
An Optimal Non-Orthogonal Separation of the Anisotropic Gaussian Convolution Filter
Keywords: Anisotropic Gaussian filter, linear filtering, orientation space, nD image processing, separable filters
(25 pages, 2005)

83. H. Andrä, D. Stoyanov
Error indicators in the parallel finite element solver for linear elasticity DDFEM
Keywords: linear elasticity, finite element method, hierarchical shape functions, domain decom-position, parallel implementation, a posteriori error estimates
(21 pages, 2006)

84. M. Schröder, I. Solchenbach
Optimization of Transfer Quality in Regional Public Transit
Keywords: public transit, transfer quality, quadratic assignment problem
(16 pages, 2006)

85. A. Naumovich, F. J. Gaspar
On a multigrid solver for the three-dimensional Biot poroelasticity system in multilayered domains
Keywords: poroelasticity, interface problem, multigrid, operator-dependent prolongation
(11 pages, 2006)

86. S. Panda, R. Wegener, N. Marheineke
Slender Body Theory for the Dynamics of Curved Viscous Fibers
Keywords: curved viscous fibers; fluid dynamics; Navier-Stokes equations; free boundary value problem; asymptotic expansions; slender body theory
(14 pages, 2006)

87. E. Ivanov, H. Andrä, A. Kudryavtsev
Domain Decomposition Approach for Automatic Parallel Generation of Tetrahedral Grids
Key words: Grid Generation, Unstructured Grid, Delaunay Triangulation, Parallel Programming, Domain Decomposition, Load Balancing
(18 pages, 2006)

88. S. Tiwari, S. Antonov, D. Hietel, J. Kuhnert, R. Wegener
A Meshfree Method for Simulations of Interactions between Fluids and Flexible Structures
Key words: Meshfree Method, FPM, Fluid Structure Interaction, Sheet of Paper, Dynamical Coupling
(16 pages, 2006)

89. R. Ciegis , O. Iliev, V. Starikovicius, K. Steiner
Numerical Algorithms for Solving Problems of Multiphase Flows in Porous Media

Keywords: nonlinear algorithms, finite-volume method, software tools, porous media, flows
(16 pages, 2006)

90. D. Niedziela, O. Iliev, A. Latz
On 3D Numerical Simulations of Viscoelastic Fluids
Keywords: non-Newtonian fluids, anisotropic viscosity, integral constitutive equation
(18 pages, 2006)

91. A. Winterfeld
Application of general semi-infinite Programming to Lapidary Cutting Problems
Keywords: large scale optimization, nonlinear programming, general semi-infinite optimization, design centering, clustering
(26 pages, 2006)

92. J. Orlik, A. Ostrovska
Space-Time Finite Element Approximation and Numerical Solution of Hereditary Linear Viscoelasticity Problems
Keywords: hereditary viscoelasticity; kern approximation by interpolation; space-time finite element approximation, stability and a priori estimate
(24 pages, 2006)

93. V. Rutka, A. Wiegmann, H. Andrä
EJIIM for Calculation of effective Elastic Moduli in 3D Linear Elasticity
Keywords: Elliptic PDE, linear elasticity, irregular domain, finite differences, fast solvers, effective elastic moduli
(24 pages, 2006)

94. A. Wiegmann, A. Zemitis
EJ-HEAT: A Fast Explicit Jump Harmonic Averaging Solver for the Effective Heat Conductivity of Composite Materials
Keywords: Stationary heat equation, effective thermal conductivity, explicit jump, discontinuous coefficients, virtual material design, microstructure simulation, EJ-HEAT
(21 pages, 2006)

95. A. Naumovich
On a finite volume discretization of the three-dimensional Biot poroelasticity system in multilayered domains
Keywords: Biot poroelasticity system, interface problems, finite volume discretization, finite difference method
(21 pages, 2006)

96. M. Krekel, J. Wenzel
A unified approach to Credit Default Swaption and Constant Maturity Credit Default Swap valuation
Keywords: LIBOR market model, credit risk, Credit Default Swaption, Constant Maturity Credit Default Swap-method
(43 pages, 2006)

97. A. Dreyer
Interval Methods for Analog Circiuts
Keywords: interval arithmetic, analog circuits, tolerance analysis, parametric linear systems, frequency response, symbolic analysis, CAD, computer algebra
(36 pages, 2006)

98. N. Weigel, S. Weihe, G. Bitsch, K. Dreßler
Usage of Simulation for Design and Optimization of Testing
Keywords: Vehicle test rigs, MBS, control, hydraulics, testing philosophy
(14 pages, 2006)

99. H. Lang, G. Bitsch, K. Dreßler, M. Speckert
Comparison of the solutions of the elastic and elastoplastic boundary value problems
Keywords: Elastic BVP, elastoplastic BVP, variational inequalities, rate-independency, hysteresis, linear kinematic hardening, stop- and play-operator
(21 pages, 2006)

100. M. Speckert, K. Dreßler, H. Mauch
MBS Simulation of a hexapod based suspension test rig
Keywords: Test rig, MBS simulation, suspension, hydraulics, controlling, design optimization
(12 pages, 2006)

101. S. Azizi Sultan, K.-H. Küfer
A dynamic algorithm for beam orientations in multicriteria IMRT planning
Keywords: radiotherapy planning, beam orientation optimization, dynamic approach, evolutionary algorithm, global optimization
(14 pages, 2006)

102. T. Götz, A. Klar, N. Marheineke, R. Wegener
A Stochastic Model for the Fiber Lay-down Process in the Nonwoven Production
Keywords: fiber dynamics, stochastic Hamiltonian system, stochastic averaging
(17 pages, 2006)

103. Ph. Süss, K.-H. Küfer
Balancing control and simplicity: a variable aggregation method in intensity modulated radiation therapy planning
Keywords: IMRT planning, variable aggregation, clustering methods
(22 pages, 2006)

104. A. Beaudry, G. Laporte, T. Melo, S. Nickel
Dynamic transportation of patients in hospitals
Keywords: in-house hospital transportation, dial-a-ride, dynamic mode, tabu search
(37 pages, 2006)

105. Th. Hanne
Applying multiobjective evolutionary algorithms in industrial projects
Keywords: multiobjective evolutionary algorithms, discrete optimization, continuous optimization, electronic circuit design, semi-infinite programming, scheduling
(18 pages, 2006)

106. J. Franke, S. Halim
Wild bootstrap tests for comparing signals and images
Keywords: wild bootstrap test, texture classification, textile quality control, defect detection, kernel estimate, nonparametric regression
(13 pages, 2007)

107. Z. Drezner, S. Nickel
Solving the ordered one-median problem in the plane
Keywords: planar location, global optimization, ordered median, big triangle small triangle method, bounds, numerical experiments
(21 pages, 2007)

108. Th. Götz, A. Klar, A. Unterreiter, R. Wegener
Numerical evidance for the non-existing of solutions of the equations desribing rotational fiber spinning
Keywords: rotational fiber spinning, viscous fibers, boundary value problem, existence of solutions
(11 pages, 2007)

109. Ph. Süss, K.-H. Küfer
Smooth intensity maps and the Bortfeld-Boyer sequencer
Keywords: probabilistic analysis, intensity modulated radiotherapy treatment (IMRT), IMRT plan application, step-and-shoot sequencing
(8 pages, 2007)

110. E. Ivanov, O. Gluchshenko, H. Andrä, A. Kudryavtsev
Parallel software tool for decomposing and meshing of 3d structures
Keywords: a-priori domain decomposition, unstructured grid, Delaunay mesh generation
(14 pages, 2007)

111. O. Iliev, R. Lazarov, J. Willems
Numerical study of two-grid preconditioners for 1d elliptic problems with highly oscillating discontinuous coefficients
Keywords: two-grid algorithm, oscillating coefficients, preconditioner
(20 pages, 2007)

112. L. Bonilla, T. Götz, A. Klar, N. Marheineke, R. Wegener
Hydrodynamic limit of the Fokker-Planck-equation describing fiber lay-down processes
Keywords: stochastic dierential equations, Fokker-Planck equation, asymptotic expansion, Ornstein-Uhlenbeck process
(17 pages, 2007)

113. S. Rief
Modeling and simulation of the pressing section of a paper machine
Keywords: paper machine, computational fluid dynamics, porous media
(41 pages, 2007)

114. R. Ciegis, O. Iliev, Z. Lakdawala
On parallel numerical algorithms for simulating industrial filtration problems
Keywords: Navier-Stokes-Brinkmann equations, finite volume discretization method, SIMPLE, parallel computing, data decomposition method
(24 pages, 2007)

115. N. Marheineke, R. Wegener
Dynamics of curved viscous fibers with surface tension
Keywords: Slender body theory, curved viscous bers with surface tension, free boundary value problem
(25 pages, 2007)

116. S. Feth, J. Franke, M. Speckert
Resampling-Methoden zur mse-Korrektur und Anwendungen in der Betriebsfestigkeit
Keywords: Weibull, Bootstrap, Maximum-Likelihood, Betriebsfestigkeit
(16 pages, 2007)

117. H. Knaf
Kernel Fisher discriminant functions – a concise and rigorous introduction
Keywords: wild bootstrap test, texture classification, textile quality control, defect detection, kernel estimate, nonparametric regression
(30 pages, 2007)

118. O. Iliev, I. Rybak
On numerical upscaling for flows in heterogeneous porous media
Keywords: numerical upscaling, heterogeneous porous media, single phase flow, Darcy's law, multiscale problem, effective permeability, multipoint flux approximation, anisotropy
(17 pages, 2007)

119. O. Iliev, I. Rybak
On approximation property of multipoint flux approximation method
Keywords: Multipoint flux approximation, finite volume method, elliptic equation, discontinuous tensor coefficients, anisotropy
(15 pages, 2007)

120. O. Iliev, I. Rybak, J. Willems
On upscaling heat conductivity for a class of industrial problems
Keywords: Multiscale problems, effective heat conductivity, numerical upscaling, domain decomposition
(21 pages, 2007)

121. R. Ewing, O. Iliev, R. Lazarov, I. Rybak
On two-level preconditioners for flow in porous media
Keywords: Multiscale problem, Darcy's law, single phase flow, anisotropic heterogeneous porous media, numerical upscaling, multigrid, domain decomposition, efficient preconditioner
(18 pages, 2007)

122. M. Brickenstein, A. Dreyer
POLYBORI: A Gröbner basis framework for Boolean polynomials
Keywords: Gröbner basis, formal verification, Boolean polynomials, algebraic cryptoanalysis, satisfiability
(23 pages, 2007)

123. O. Wirjadi
Survey of 3d image segmentation methods
Keywords: image processing, 3d, image segmentation, binarization
(20 pages, 2007)

124. S. Zeytun, A. Gupta
A Comparative Study of the Vasicek and the CIR Model of the Short Rate
Keywords: interest rates, Vasicek model, CIR-model, calibration, parameter estimation
(17 pages, 2007)

125. G. Hanselmann, A. Sarishvili
Heterogeneous redundancy in software quality prediction using a hybrid Bayesian approach
Keywords: reliability prediction, fault prediction, non-homogeneous poisson process, Bayesian model averaging
(17 pages, 2007)

126. V. Maag, M. Berger, A. Winterfeld, K.-H. Küfer
A novel non-linear approach to minimal area rectangular packing
Keywords: rectangular packing, non-overlapping constraints, non-linear optimization, regularization, relaxation
(18 pages, 2007)

127. M. Monz, K.-H. Küfer, T. Bortfeld, C. Thieke
Pareto navigation – systematic multi-criteria-based IMRT treatment plan determination
Keywords: convex, interactive multi-objective optimization, intensity modulated radiotherapy planning
(15 pages, 2007)

128. M. Krause, A. Scherrer
On the role of modeling parameters in IMRT plan optimization
Keywords: intensity-modulated radiotherapy (IMRT), inverse IMRT planning, convex optimization, sensitivity analysis, elasticity, modeling parameters, equivalent uniform dose (EUD)
(18 pages, 2007)

129. A. Wiegmann
Computation of the permeability of porous materials from their microstructure by FFF-Stokes
Keywords: permeability, numerical homogenization, fast Stokes solver
(24 pages, 2007)

130. T. Melo, S. Nickel, F. Saldanha da Gama
Facility Location and Supply Chain Management – A comprehensive review
Keywords: facility location, supply chain management, network design
(54 pages, 2007)

131. T. Hanne, T. Melo, S. Nickel
Bringing robustness to patient flow management through optimized patient transports in hospitals
Keywords: Dial-a-Ride problem, online problem, case study, tabu search, hospital logistics
(23 pages, 2007)

132. R. Ewing, O. Iliev, R. Lazarov, I. Rybak, J. Willems
An efficient approach for upscaling properties of composite materials with high contrast of coefficients
Keywords: effective heat conductivity, permeability of fractured porous media, numerical upscaling, fibrous insulation materials, metal foams
(16 pages, 2008)

133. S. Gelareh, S. Nickel
New approaches to hub location problems in public transport planning
Keywords: integer programming, hub location, transportation, decomposition, heuristic
(25 pages, 2008)

134. G. Thömmes, J. Becker, M. Junk, A. K. Vaikuntam, D. Kehrwald, A. Klar, K. Steiner, A. Wiegmann
A Lattice Boltzmann Method for immiscible multiphase flow simulations using the Level Set Method
Keywords: Lattice Boltzmann method, Level Set method, free surface, multiphase flow
(28 pages, 2008)

135. J. Orlik
Homogenization in elasto-plasticity
Keywords: multiscale structures, asymptotic homogenization, nonlinear energy
(40 pages, 2008)

136. J. Almquist, H. Schmidt, P. Lang, J. Deitmer, M. Jirstrand, D. Prätzel-Wolters, H. Becker
Determination of interaction between MCT1 and CAII via a mathematical and physiological approach
Keywords: mathematical modeling; model reduction; electrophysiology; pH-sensitive microelectrodes; proton antenna
(20 pages, 2008)

137. E. Savenkov, H. Andrä, O. Iliev
An analysis of one regularization approach for solution of pure Neumann problem
Keywords: pure Neumann problem, elasticity, regularization, finite element method, condition number
(27 pages, 2008)

138. O. Berman, J. Kalcsics, D. Krass, S. Nickel
The ordered gradual covering location problem on a network
Keywords: gradual covering, ordered median function, network location
(32 pages, 2008)

139. S. Gelareh, S. Nickel
Multi-period public transport design: A novel model and solution approaches
Keywords: Integer programming, hub location, public transport, multi-period planning, heuristics
(31 pages, 2008)

140. T. Melo, S. Nickel, F. Saldanha-da-Gama
Network design decisions in supply chain planning
Keywords: supply chain design, integer programming models, location models, heuristics
(20 pages, 2008)

141. C. Lautensack, A. Särkkä, J. Freitag, K. Schladitz
Anisotropy analysis of pressed point processes
Keywords: estimation of compression, isotropy test, nearest neighbour distance, orientation analysis, polar ice, Ripley's K function
(35 pages, 2008)

142. O. Iliev, R. Lazarov, J. Willems
A Graph-Laplacian approach for calculating the effective thermal conductivity of complicated fiber geometries
Keywords: graph laplacian, effective heat conductivity, numerical upscaling, fibrous materials
(14 pages, 2008)

143. J. Linn, T. Stephan, J. Carlsson, R. Bohlin
Fast simulation of quasistatic rod deformations for VR applications
Keywords: quasistatic deformations, geometrically exact rod models, variational formulation, energy minimization, finite differences, nonlinear conjugate gradients
(7 pages, 2008)

144. J. Linn, T. Stephan
Simulation of quasistatic deformations using discrete rod models
Keywords: quasistatic deformations, geometrically exact rod models, variational formulation, energy minimization, finite differences, nonlinear conjugate gradients
(9 pages, 2008)

145. J. Marburger, N. Marheineke, R. Pinnau
Adjoint based optimal control using meshless discretizations
Keywords: Mesh-less methods, particle methods, Eulerian-Lagrangian formulation, optimization strategies, adjoint method, hyperbolic equations
(14 pages, 2008

146. S. Desmettre, J. Gould, A. Szimayer
Own-company stockholding and work effort preferences of an unconstrained executive
Keywords: optimal portfolio choice, executive compensation
(33 pages, 2008)

147. M. Berger, M. Schröder, K.-H. Küfer
A constraint programming approach for the two-dimensional rectangular packing problem with orthogonal orientations
Keywords: rectangular packing, orthogonal orientations non-overlapping constraints, constraint propagation
(13 pages, 2008)

148. K. Schladitz, C. Redenbach, T. Sych, M. Godehardt
Microstructural characterisation of open foams using 3d images
Keywords: virtual material design, image analysis, open foams
(30 pages, 2008)

149. E. Fernández, J. Kalcsics, S. Nickel, R. Ríos-Mercado
A novel territory design model arising in the implementation of the WEEE-Directive
Keywords: heuristics, optimization, logistics, recycling
(28 pages, 2008)

150. H. Lang, J. Linn
Lagrangian field theory in space-time for geometrically exact Cosserat rods
Keywords: Cosserat rods, geometrically exact rods, small strain, large deformation, deformable bodies, Lagrangian field theory, variational calculus
(19 pages, 2009)

151. K. Dreßler, M. Speckert, R. Müller, Ch. Weber
Customer loads correlation in truck engineering
Keywords: Customer distribution, safety critical components, quantile estimation, Monte-Carlo methods
(11 pages, 2009)

152. H. Lang, K. Dreßler
An improved multiaxial stress-strain correction model for elastic FE postprocessing
Keywords: Jiang's model of elastoplasticity, stress-strain correction, parameter identification, automatic differentiation, least-squares optimization, Coleman-Li algorithm
(6 pages, 2009)

153. J. Kalcsics, S. Nickel, M. Schröder
A generic geometric approach to territory design and districting
Keywords: Territory design, districting, combinatorial optimization, heuristics, computational geometry
(32 pages, 2009)

154. Th. Fütterer, A. Klar, R. Wegener
An energy conserving numerical scheme for the dynamics of hyperelastic rods
Keywords: Cosserat rod, hyperealstic, energy conservation, finite differences
(16 pages, 2009)

155. A. Wiegmann, L. Cheng, E. Glatt, O. Iliev, S. Rief
Design of pleated filters by computer simulations
Keywords: Solid-gas separation, solid-liquid separation, pleated filter, design, simulation
(21 pages, 2009)

156. A. Klar, N. Marheineke, R. Wegener
Hierarchy of mathematical models for production processes of technical textiles
Keywords: Fiber-fluid interaction, slender-body theory, turbulence modeling, model reduction, stochastic differential equations, Fokker-Planck equation, asymptotic expansions, parameter identification
(21 pages, 2009)

157. E. Glatt, S. Rief, A. Wiegmann, M. Knefel, E. Wegenke
Structure and pressure drop of real and virtual metal wire meshes
Keywords: metal wire mesh, structure simulation, model calibration, CFD simulation, pressure loss
(7 pages, 2009)

158. S. Kruse, M. Müller
Pricing American call options under the assumption of stochastic dividends – An application of the Korn-Rogers model
Keywords: option pricing, American options, dividends, dividend discount model, Black-Scholes model
(22 pages, 2009)

159. H. Lang, J. Linn, M. Arnold
Multibody dynamics simulation of geometrically exact Cosserat rods
Keywords: flexible multibody dynamics, large deformations, finite rotations, constrained mechanical systems, structural dynamics
(20 pages, 2009)

160. P. Jung, S. Leyendecker, J. Linn, M. Ortiz
Discrete Lagrangian mechanics and geometrically exact Cosserat rods
Keywords: special Cosserat rods, Lagrangian mechanics, Noether's theorem, discrete mechanics, frame-indifference, holonomic constraints
(14 pages, 2009)

161. M. Burger, K. Dreßler, A. Marquardt, M. Speckert
Calculating invariant loads for system simulation in vehicle engineering
Keywords: iterative learning control, optimal control theory, differential algebraic equations (DAEs)
(18 pages, 2009)

162. M. Speckert, N. Ruf, K. Dreßler
Undesired drift of multibody models excited by measured accelerations or forces
Keywords: multibody simulation, full vehicle model, force-based simulation, drift due to noise
(19 pages, 2009)

163. A. Streit, K. Dreßler, M. Speckert, J. Lichter, T. Zenner, P. Bach
Anwendung statistischer Methoden zur Erstellung von Nutzungsprofilen für die Auslegung von Mobilbaggern
Keywords: Nutzungsvielfalt, Kundenbeanspruchung, Bemessungsgrundlagen
(13 pages, 2009)

164. I. Correia, S. Nickel, F. Saldanha-da-Gama
The capacitated single-allocation hub location problem revisited: A note on a classical formulation
Keywords: Capacitated Hub Location, MIP formulations
(10 pages, 2009)

165. F. Yaneva, T. Grebe, A. Scherrer
An alternative view on global radiotherapy optimization problems
Keywords: radiotherapy planning, path-connected sublevelsets, modified gradient projection method, improving and feasible directions
(14 pages, 2009)

166. J. I. Serna, M. Monz, K.-H. Küfer, C. Thieke
Trade-off bounds and their effect in multi-criteria IMRT planning
Keywords: trade-off bounds, multi-criteria optimization, IMRT, Pareto surface
(15 pages, 2009)

167. W. Arne, N. Marheineke, A. Meister, R. Wegener
Numerical analysis of Cosserat rod and string models for viscous jets in rotational spinning processes
Keywords: Rotational spinning process, curved viscous fibers, asymptotic Cosserat models, boundary value problem, existence of numerical solutions
(18 pages, 2009)

168. T. Melo, S. Nickel, F. Saldanha-da-Gama
An LP-rounding heuristic to solve a multi-period facility relocation problem
Keywords: supply chain design, heuristic, linear programming, rounding
(37 pages, 2009)

169. I. Correia, S. Nickel, F. Saldanha-da-Gama
Single-allocation hub location problems with capacity choices
Keywords: hub location, capacity decisions, MILP formulations
(27 pages, 2009)

170. S. Acar, K. Natcheva-Acar
A guide on the implementation of the Heath-Jarrow-Morton Two-Factor Gaussian Short Rate Model (HJM-G2++)
Keywords: short rate model, two factor Gaussian, G2++, option pricing, calibration
(30 pages, 2009)

171. A. Szimayer, G. Dimitroff, S. Lorenz
A parsimonious multi-asset Heston model: calibration and derivative pricing
Keywords: Heston model, multi-asset, option pricing, calibration, correlation
(28 pages, 2009)

172. N. Marheineke, R. Wegener
Modeling and validation of a stochastic drag for fibers in turbulent flows
Keywords: fiber-fluid interactions, long slender fibers, turbulence modelling, aerodynamic drag, dimensional analysis, data interpolation, stochastic partial differential algebraic equation, numerical simulations, experimental validations
(19 pages, 2009)

173. S. Nickel, M. Schröder, J. Steeg
Planning for home health care services
Keywords: home health care, route planning, metaheuristics, constraint programming
(23 pages, 2009)

174. G. Dimitroff, A. Szimayer, A. Wagner
Quanto option pricing in the parsimonious Heston model
Keywords: Heston model, multi asset, quanto options, option pricing
(14 pages, 2009)

175. S. Herkt, K. Dreßler, R. Pinnau
Model reduction of nonlinear problems in structural mechanics
Keywords: flexible bodies, FEM, nonlinear model reduction, POD
(13 pages, 2009)

176. M. K. Ahmad, S. Didas, J. Iqbal
Using the Sharp Operator for edge detection and nonlinear diffusion
Keywords: maximal function, sharp function,image processing, edge detection, nonlinear diffusion
(17 pages, 2009)

177. M. Speckert, N. Ruf, K. Dreßler, R. Müller, C. Weber, S. Weihe
Ein neuer Ansatz zur Ermittlung von Erprobungslasten für sicherheitsrelevante Bauteile
Keywords: sicherheitsrelevante Bauteile, Kundenbeanspruchung, Festigkeitsverteilung, Ausfallwahrscheinlichkeit, Konfidenz, statistische Unsicherheit, Sicherheitsfaktoren
(16 pages, 2009)

178. J. Jegorovs
Wave based method: new applicability areas
Keywords: Elliptic boundary value problems, inhomogeneous Helmholtz type differential equations in bounded domains, numerical methods, wave based method, uniform B-splines
(10 pages, 2009)

179. H. Lang, M. Arnold
Numerical aspects in the dynamic simulation of geometrically exact rods
Keywords: Kirchhoff and Cosserat rods, geometrically exact rods, deformable bodies, multibody dynamics,artial differential algebraic equations, method of lines, time integration
(21 pages, 2009)

180. H. Lang
Comparison of quaternionic and rotation-free null space formalisms for multibody dynamics
Keywords: Parametrisation of rotations, differential-algebraic equations, multibody dynamics, constrained mechanical systems, Lagrangian mechanics
(40 pages, 2010)

181. S. Nickel, F. Saldanha-da-Gama, H.-P. Ziegler
Stochastic programming approaches for risk aware supply chain network design problems
Keywords: Supply Chain Management, multi-stage stochastic programming, financial decisions, risk
(37 pages, 2010)

182. P. Ruckdeschel, N. Horbenko
Robustness properties of estimators in generalized Pareto Models
Keywords: global robustness, local robustness, finite sample breakdown point, generalized Pareto distribution
(58 pages, 2010)

183. P. Jung, S. Leyendecker, J. Linn, M. Ortiz
A discrete mechanics approach to Cosserat rod theory – Part 1: static equilibria
Keywords: Special Cosserat rods; Lagrangian mechanics; Noether's theorem; discrete mechanics; frame-indifference; holonomic constraints; variational formulation
(35 pages, 2010)

184. R. Eymard, G. Printsypar
A proof of convergence of a finite volume scheme for modified steady Richards' equation describing transport processes in the pressing section of a paper machine
Keywords: flow in porous media, steady Richards' equation, finite volume methods, convergence of approximate solution
(14 pages, 2010)

185. P. Ruckdeschel
Optimally Robust Kalman Filtering
Keywords: robustness, Kalman Filter, innovation outlier, additive outlier
(42 pages, 2010)

186. S. Repke, N. Marheineke, R. Pinnau
On adjoint-based optimization of a free surface Stokes flow
Keywords: film casting process, thin films, free surface Stokes flow, optimal control, Lagrange formalism
(13 pages, 2010)

187. O. Iliev, R. Lazarov, J. Willems
Variational multiscale Finite Element Method for flows in highly porous media
Keywords: numerical upscaling, flow in heterogeneous porous media, Brinkman equations, Darcy's law, subgrid approximation, discontinuous Galerkin mixed FEM
(21 pages, 2010)

188. S. Desmettre, A. Szimayer
Work effort, consumption, and portfolio selection: When the occupational choice matters
Keywords: portfolio choice, work effort, consumption, occupational choice
(34 pages, 2010)

189. O. Iliev, Z. Lakdawala, V. Starikovicius
On a numerical subgrid upscaling algorithm for Stokes-Brinkman equations
Keywords: Stokes-Brinkman equations, subgrid approach, multiscale problems, numerical upscaling
(27 pages, 2010)

190. A. Latz, J. Zausch, O. Iliev
Modeling of species and charge transport in Li-Ion Batteries based on non-equilibrium thermodynamics
Keywords: lithium-ion battery, battery modeling, electrochemical simulation, concentrated electrolyte, ion transport
(8 pages, 2010)

191. P. Popov, Y. Vutov, S. Margenov, O. Iliev
Finite volume discretization of equations describing nonlinear diffusion in Li-Ion batteries
Keywords: nonlinear diffusion, finite volume discretization, Newton method, Li-Ion batteries
(9 pages, 2010)

192. W. Arne, N. Marheineke, R. Wegener
Asymptotic transition from Cosserat rod to string models for curved viscous inertial jets
Keywords: rotational spinning processes; inertial and viscous-inertial fiber regimes; asymptotic limits; slender-body theory; boundary value problems
(23 pages, 2010)

193. L. Engelhardt, M. Burger, G. Bitsch
Real-time simulation of multibody-systems for on-board applications
Keywords: multibody system simulation, real-time simulation, on-board simulation, Rosenbrock methods
(10 pages, 2010)

194. M. Burger, M. Speckert, K. Dreßler
Optimal control methods for the calculation of invariant excitation signals for multibody systems
Keywords: optimal control, optimization, mbs simulation, invariant excitation
(9 pages, 2010)

195. A. Latz, J. Zausch
Thermodynamic consistent transport theory of Li-Ion batteries
Keywords: Li-Ion batteries, nonequilibrium thermodynamics, thermal transport, modeling
(18 pages, 2010)

196. S. Desmettre
Optimal investment for executive stockholders with exponential utility
Keywords: portfolio choice, executive stockholder, work effort, exponential utility
(24 pages, 2010)

197. W. Arne, N. Marheineke, J. Schnebele, R. Wegener
Fluid-fiber-interactions in rotational spinning process of glass wool production
Keywords: Rotational spinning process, viscous thermal jets, fluid-fiber-interactions, two-way coupling, slender-body theory, Cosserat rods, drag models, boundary value problem, continuation method
(20 pages, 2010)

198. A. Klar, J. Maringer, R. Wegener
A 3d model for fiber lay-down in nonwoven production processes
Keywords: fiber dynamics, Fokker-Planck equations, diffusion limits
(15 pages, 2010)

199. Ch. Erlwein, M. Müller
A regime-switching regression model for hedge funds
Keywords: switching regression model, Hedge funds, optimal parameter estimation, filtering
(26 pages, 2011)

200. M. Dalheimer
Power to the people – Das Stromnetz der Zukunft
Keywords: Smart Grid, Stromnetz, Erneuerbare Energien, Demand-Side Management
(27 pages, 2011)

201. D. Stahl, J. Hauth
PF-MPC: Particle Filter-Model Predictive Control
Keywords: Model Predictive Control, Particle Filter, CSTR, Inverted Pendulum, Nonlinear Systems, Sequential Monte Carlo
(40 pages, 2011)

202. G. Dimitroff, J. de Kock
Calibrating and completing the volatility cube in the SABR Model
Keywords: stochastic volatility, SABR, volatility cube, swaption
(12 pages, 2011)

203. J.-P. Kreiss, T. Zangmeister
Quantification of the effectiveness of a safety function in passenger vehicles on the basis of real-world accident data
Keywords: logistic regression, safety function, real-world accident data, statistical modeling
(23 pages, 2011)

204. P. Ruckdeschel, T. Sayer, A. Szimayer
Pricing American options in the Heston model: a close look on incorporating correlation
Keywords: Heston model, American options, moment matching, correlation, tree method
(30 pages, 2011)

205. H. Ackermann, H. Ewe, K.-H. Küfer, M. Schröder
Modeling profit sharing in combinatorial exchanges by network flows
Keywords: Algorithmic game theory, profit sharing, combinatorial exchange, network flows, budget balance, core
(17 pages, 2011)

206. O. Iliev, G. Printsypar, S. Rief
A one-dimensional model of the pressing section of a paper machine including dynamic capillary effects
Keywords: steady modified Richards' equation, finite volume method, dynamic capillary pressure, pressing section of a paper machine
(29 pages, 2011)

207. I. Vecchio, K. Schladitz, M. Godehardt, M. J. Heneka
Geometric characterization of particles in 3d with an application to technical cleanliness
Keywords: intrinsic volumes, isoperimetric shape factors, bounding box, elongation, geodesic distance, technical cleanliness
(21 pages, 2011)

208. M. Burger, K. Dreßler, M. Speckert
Invariant input loads for full vehicle multibody system simulation
Keywords: multibody systems, full-vehicle simulation, optimal control
(8 pages, 2011)

209. H. Lang, J. Linn, M. Arnold
Multibody dynamics simulation of geometrically exact Cosserat rods
Keywords: flexible multibody dynamics, large deformations, finite rotations, constrained mechanical systems, structural dynamics
(28 pages, 2011)

210. G. Printsypar, R. Ciegis
On convergence of a discrete problem describing transport processes in the pressing section of a paper machine including dynamic capillary effects: one-dimensional case
Keywords: saturated and unsaturated fluid flow in porous media, Richards' approach, dynamic capillary pressure, finite volume methods, convergence of approximate solution
(24 pages, 2011)

211. O. Iliev, G. Printsypar, S. Rief
A two-cimensional model of the pressing section of a paper machine including dynamic capillary effects
Keywords: two-phase flow in porous media, steady modified Richards' equation, finite volume method, dynamic capillary pressure, pressing section of a paper machine, multipoint flux approximation
(44 pages, 2012)

212. M. Buck, O. Iliev, H. Andrä
Multiscale finite element coarse spaces for the analysis of linear elastic composites
Keywords: linear elasticity, domain decomposition, multiscale finite elements, robust coarse spaces, rigid body modes, discontinuous coefficients
(31 pages, 2012)

213. A. Wagner
Residual demand modeling and application to electricity pricing
Keywords: residual demand modeling, renewable infeed, wind infeed, solar infeed, electricity demand, German power market, merit-order effect
(28 pages, 2012)

214. O. Iliev, A. Latz, J. Zausch, S. Zhang
An overview on the usage of some model reduction approaches for simulations of Li-ion transport in batteries
Keywords: Li-ion batteries, porous electrode model, model reduction
(21 pages, 2012)

215. C. Zémerli, A. Latz, H. Andrä
Constitutive models for static granular systems and focus to the Jiang-Liu hyperelastic law
Keywords: granular elasticity, constitutive modelling, non-linear finite element method
(33 pages, 2012)

216. T. Gornak, J. L. Guermond, O. Iliev, P. D. Minev
A direction splitting approach for incompressible Brinkmann flow
Keywords: unsteady Navier-Stokes-Brinkman equations, direction splitting algorithms, nuclear reactors safety simulations
(16 pages, 2012)

217. Y. Efendiev, O. Iliev, C. Kronsbein
Multilevel Monte Carlo methods using ensemble level mixed MsFEM for two-phase flow and transport simulations
Keywords: two phase flow in porous media, uncertainty quantification, multilevel Monte Carlo
(28 pages, 2012)

218. J. Linn, H. Lang, A. Tuganov
Geometrically exact Cosserat rods with Kelvin-Voigt type viscous damping
Keywords: geometrically exact rods, viscous damping, Kelvin-Voigt model, material damping parameters
(10 pages, 2012)

219. M. Schulze, S. Dietz, J. Linn, H. Lang, A. Tuganov
Integration of nonlinear models of flexible body deformation in Multibody System Dynamics
Keywords: multibody system dynamics, flexible structures, discrete Cosserat rods, wind turbine rotor blades
(10 pages, 2012)

220. C. Weischedel, A. Tuganov, T. Hermansson, J. Linn, M. Wardetzky
Construction of discrete shell models by geometric finite differences
Keywords: geometrically exact shells, discrete differential geometry, rotation-free Kirchhoff model, triangular meshes
(10 pages, 2012)

221. M. Taralov, V. Taralova, P. Popov, O. Iliev, A. Latz, J. Zausch
Report on Finite Element Simulations of Electrochemical Processes in Li-ion Batteries with Thermic Effects
Keywords: Li-ion battery, FEM for nonlinear problems, FEM for discontinuous solutions, Nonlinear diffusion, Nonlinear interface conditions
(40 pages, 2012)

222. A. Scherrer, T. Grebe, F. Yaneva, K.-H. Küfer
Interactive DVH-based planning of intensity-modulated radiation therapy (IMRT)
Keywords: intensity-modulated radiation therapy (IMRT), cumulative dose-volume histogram (DVH), interactive IMRT planning, DVH-based planning criteria
(22 pages, 2012)

223. S. Frei, H. Andrä, R. Pinnau, O. Tse
An adjoint-based gradient-type algorithm for optimal fiber orientation in fiber-reinforced materials
Keywords: pde constrained optimization, fiber-reinforced materials, fiber orientation, linear elasticity, upscaling, adjoint-based optimization, microstructural optimization
(17 pages, 2012)

224. M. Kabel, H. Andrä
Fast numerical computation of precise bounds of effective elastic moduli
Keywords: composite materials, numerical homogenization, effective elasticity coefficients, Hashin-Shtrikman bounds, Lippmann-Schwinger equation, FFT
(16 pages, 2013)

225. J. Linn, H. Lang, A. Tuganov
Derivation of a viscoelastic constitutive model of Kelvin-Voigt type for Cosserat rods
Keywords: geometrically exact rods, viscoelasticity, Kelvin-Voigt model, nonlinear structural dynamics
(42 pages, 2013)

226. H. Knaf
Distanzen zwischen Partitionen – zur Anwendung und Theorie
Keywords: Metrik, Partitionenverband, Clusteranalyse, Ergebnisbewertung
(35 pages, 2013)

227. S. Desmettre, R. Korn, F. Th. Seifried
Worst-case consumption-portfolio optimization
Keywords: worst-case, crash, consumption, verification
(30 pages, 2013)

228. M. Obermayr, Ch. Vrettos, J. Kleinert, P. Eberhard
A Discrete Element Method for assessing reaction forces in excavation tools
Keywords: discrete element method, rolling resistance, cohesionless soil, draft force
(17 pages, 2013)

229. S. Schmidt, L. Kreußer, S. Zhang
POD-DEIM based model order reduction for a three-dimensional microscopic Li-Ion battery model
Keywords: Model order reduction, nonlinear PDE, POD-DEIM, Li-Ion battery simulation
(33 pages, 2013)

230. Y. Efendiev, O. Iliev, V. Taralova
Upscaling of an isothermal Li-ion battery model via the Homogenization Theory
Keywords: Li-Ion batteries, homogenization
(66 pages, 2013)

231. D. Neusius, S. Schmidt;
A Cartesian cut-cell method for the isothermal compressible viscous Navier-Stokes Equations
Keywords: Immersed boundary methods, Cartesian cut-cell method, Finite-volume method, Compressible Navier-Stokes equations
(35 pages, 2013)

232. S. Desmettre, R. Korn, P. Ruckdeschel, F. Th. Seifried
Robust worst-case optimal investment
Keywords: worst-case, crash scenario, robust optimization, Knightian uncertainty, efficiency, min-max approach
(24 pages, 2013)

233. A. Scherrer, P. Rüdiger, A. Dinges, K.-H. Küfer, I. Schwidde, S. Kümmel
A decision support system for advanced treatment planning for breast cancer
Keywords: breast cancer therapy, disease modeling, mathematical decision making, decision support systems
(7 pages, 2013)

234. A. Hoffmann A. Scherrer, K.-H. Küfer
Analyzing the quality robustness of chemotherapy plans with respect to model uncertainties
Keywords: chemotherapy planning, ordinary differential equations, nonlinear optimization, multi-criteria decision making, sensitivity analysis, elasticity analysis
(20 pages, 2013)

235. T. Gornak
A goal oriented survey on immersed boundary methods
Keywords: immersed boundary method, survey, fictitious domain method, containment pool simulation
(23 pages, 2013)

236. T. Gornak, P. Minev, A. Zemitis
On a fast algorithm and software for 3D simulation of thermal stratification in containment pools of nuclear power plants
Keywords: Navier-Stokes equations, thermal convection (fluid dynamics), heat conduction, numerical methods, domain decomposition method, nuclear reactors safety
(15 pages, 2013)

237. A. Scherrer, I. Schwidde, A. Dinges, P. Rüdiger, S. Kümmel, K.-H. Küfer
Breast cancer therapy planning – a sequential decision making problem
Keywords: breast cancer therapy planning, sequential decision making, mathematical decision support
(17 pages, 2013)

238. J. Kleinert, M. Obermayr, M. Balzer
Modeling of large scale granular systems using the Discrete Element Method and the Non-Smooth Contact Dynamics Method: A comparison
Keywords: DEM, granular material, complementarity systems, non-smooth contact dynamics
(10 pages, 2013)

239. H. Lang, S. Leyendecker, J. Linn
Numerical experiments for viscoelastic Cosserat rods with Kelvin-Voigt damping
Keywords: Flexible multibody dynamics, geometrically exact rods, Kelvin-Voigt damping, viscoelasticity
(10 pages, 2013)

240. M. Roller, P. Betsch, A. Gallrein, J. Linn
On the use of geometrically exact shells for dynamic tire simulation
Keywords: geometrically exact shell, multibody dynamics, large rotations, dynamical contact, tire simulation
(10 pages, 2013)

241. O. Iliev, Y. Maday, T. Nagapetyan
A two-grid infinite-volume/reduced basis scheme for the approximation of the solution of parameter dependent PDE with applications to AFFFF Devices
Keywords: asymmetric flow field flow fractionation, mean exit time, finite volume, reduced basis
(14 pages, 2014)

242. M. Kleer, A. Gizatullin, K. Dreßler, S. Müller
Real-time human in the loop MBS simulation in the Fraunhofer Robot-Based Driving Simulator
Keywords: Driving simulator; human in the loop; real-time MBS simulation
(14 pages, 2014)

243. O. Bauchau, Z. Lao, M. Lyu, S. Brändle, J. Linn
Formulations of viscoelastic constitutive laws for beams in flexible multibody dynamics
Keywords: geometrically exact rods, viscoelastic materials, generalized Maxwell model, flexible multibody dynamics
(12 pages, 2014)

244. J. Kleinert, B. Simeon, M. Obermayr
An inexact Interior Point Method for the simulation of large scale granular systems
Keywords: Non-smooth dynamical systems, granular material, cone complementarity problem, symmetric cones, Interior Point Method, Jordan Algebra
(21 pages, 2014)

245. E. Di Nicolo, O. Iliev, K. H. L. Leonard
Virtual generation of microfiltration membrane geometry for the numerical simulation of contaminant transport
Keywords: Membrane, water purification, pore-scale reactive transport, mathematical model, numerical simulation
(13 pages, 2015)

246. S. Desmettre, S. Grün, F. Th. Seifried
Forecasting discrete dividends by no-arbitrage
Keywords: dividends, prediction, arbitrage, put-call parity, market-implied discount curve
(15 pages, 2015)

247. A. Scherrer, S. Jakobsson, K.-H. Küfer
On the advancement and software support of decision making in focused ultrasound therapy
Keywords: focused ultrasound, multi-criteria optimization, decision support systems
(26 pages, 2015)

248. T. Hofmann, R. Müller, H. Andrä, J. Zausch
Numerical simulation of phase separation in cathode materials of lithium ion batteries
Keywords: phase-eld model, Cahn-Hilliard equation, Butler-Volmer kinetics, intercalation, lithium-ion battery
(35 pages, 2016)

Status quo: March 2016